

Report No. CG-D-30-94

# THE DETECTION OF OIL SLICKS AT NIGHT WITH AIRBORNE INFRARED IMAGERS

**G.M. DANIELS**

Lincoln Laboratory  
Massachusetts Institute of Technology  
244 Wood Street  
Lexington, Massachusetts 02173-9108

**AND**

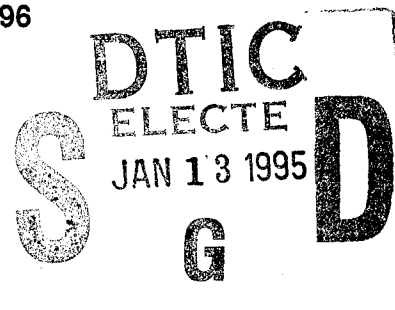
**G.L. HOVER**

U.S. Coast Guard Research And Development Center  
1082 Shennecossett Road  
Groton, Connecticut 06340-6096



**FINAL REPORT**

**DECEMBER 1994**



This document is available to the U.S. public through the  
National Technical Information Service, Springfield, Virginia 22161

Prepared for :

*THIS QUALITY REPRODUCED*

**U.S. Department of Transportation  
United States Coast Guard**

Office of Engineering, Logistics, and Development  
Washington, DC 20593

19950112 042

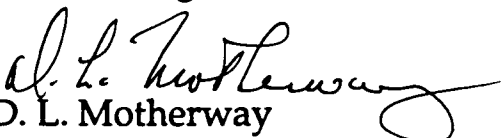
# NOTICE

This document is disseminated under the sponsorship of the Department of Transportation in the interest of information exchange. The United States Government assumes no liability for its contents or use thereof.

The United States Government does not endorse products or manufacturers. Trade or manufacturers' names appear herein solely because they are considered essential to the object of this report.

The contents of this report reflect the views of the Coast Guard Research & Development Center. This report does not constitute a standard, specification, or regulation.



  
D. L. Motherway  
Technical Director, Acting  
United States Coast Guard  
Research & Development Center  
1082 Shennecossett Road  
Groton, CT 06340-6096

Technical Report Documentation Page

1. Report No. <b>CG-D-30-94</b>		2. Government Accession No.		3. Recipient's Catalog No.	
4. Title and Subtitle <b>The Detection of Oil Slicks at Night with Airborne Infrared Imagers</b>				5. Report Date <b>December 1994</b>	
				6. Performing Organization Code	
7. Author(s) <b>G.M. Daniels and G.L. Hoyer</b>				8. Performing Organization Report No. <b>R&amp;DC 24/94</b>	
9. Performing Organization Name and Address <b>USCG R&amp;D Center 1082 Shennecossett Road Groton, CT 06340-6096</b> <b>MIT Lincoln Laboratory Massachusetts Institute of Tech 244 Wood Street Lexington, MA 02173-9108</b>				10. Work Unit No. (TRAVIS)	
				11. Contract or Grant No. <b>F19628-90-C-0002</b>	
12. Sponsoring Agency Name and Address <b>Department of Transportation U.S. Coast Guard Office of Engineering and Development Washington, DC 20593</b>				13. Type of Report and Period Covered <b>Final October 1993 - April 1994</b>	
				14. Sponsoring Agency Code	
15. Supplementary Notes					
16. Abstract The detection of oil slicks on the ocean is a Coast Guard priority. Daytime detection in clear weather is routine; but nighttime detection requires sophisticated imaging sensors. Infrared imagers have demonstrated some capability to detect oil slicks at night in the marine environment. Infrared imagers sense the thermal radiation, and its variations, in a scene rather than the reflected radiation. Gimbal-mounted thermal imagers operating in the 8-12 micron region are currently flown on Coast Guard aircraft. This study compared the performance of these imagers with hand-held imagers operating in the 3-5 micron region. The comparison was primarily theoretical with semi-quantitative support from an uncalibrated data base of infrared images taken with various sensors. It was found theoretically, and supported by image data, that the 8-12 micron instruments produced images with better water-oil contrast at night. This differential behavior was theoretically predicted to hold over a wide range of environmental conditions. The differential behavior was traced to the fact that the optical properties of water and oil are more different in the 8-12 than in the 3-5 micron bands. The utility of night-vision imagers or low-light level TVs was also assessed. Calculations indicated that typical water-oil contrasts would not be seen with current sensors. Image data appearing to contradict this conclusion was found to be defective in the sense that the conditions of the experiments were not representative of operational conditions. It is recommended that: the use of 8-12 micron imagers be continued for oil slick searches at night and the potential of new nighttime imaging devices be assessed.					
17. Key Words <b>Oil Slick Detection, Infrared, Oil Spill Sensing, Nighttime Sensing</b>			18. Distribution Statement <b>Document is available to the U.S. public through the National Information Service, Springfield, MA 22161</b> <b>DTIC QUALITY INSPECTED 3</b>		
19. Security Classif. (of this report) <b>Unclassified</b>		20. SECURITY CLASSIF. (of this page) <b>Unclassified</b>		21. No. of Pages <b>83</b>	22. Price

# METRIC CONVERSION FACTORS

## Approximate Conversions to Metric Measures

Symbol	When You Know	Multiply By	To Find	Symbol
<b>LENGTH</b>				
in	inches	* 2.5	centimeters	cm
ft	feet	30	centimeters	cm
yd	yards	0.9	meters	m
mi	miles	1.6	kilometers	km
<b>AREA</b>				
in <sup>2</sup>	square inches	6.5	square centimeters	cm <sup>2</sup>
ft <sup>2</sup>	square feet	0.09	square meters	m <sup>2</sup>
yd <sup>2</sup>	square yards	0.8	square meters	m <sup>2</sup>
mi <sup>2</sup>	square miles	2.6	square kilometers	km <sup>2</sup>
	acres	0.4	hectares	ha
<b>MASS (WEIGHT)</b>				
oz	ounces	28	grams	g
lb	pounds	0.45	kilograms	kg
	short tons (2000 lb)	0.9	tonnes	t
<b>VOLUME</b>				
tsp	teaspoons	5	milliliters	ml
tbsp	tablespoons	15	milliliters	ml
fl oz	fluid ounces	30	milliliters	ml
c	cups	0.24	liters	l
pt	pints	0.47	liters	l
qt	quarts	0.95	liters	l
gal	gallons	3.8	liters	l
ft <sup>3</sup>	cubic feet	0.03	cubic meters	m <sup>3</sup>
yd <sup>3</sup>	cubic yards	0.76	cubic meters	m <sup>3</sup>
<b>TEMPERATURE (EXACT)</b>				
°F	Fahrenheit temperature	5/9 (after subtracting 32)	Celsius temperature	°C

\* 1 in = 2.54 (exactly).

## Approximate Conversions from Metric Measures

Symbol	When You Know	Multiply By	To Find	Symbol
<b>LENGTH</b>				
mm	millimeters	0.04	inches	in
cm	centimeters	0.4	inches	in
m	meters	3.3	feet	ft
m	meters	1.1	yards	yd
km	kilometers	0.6	miles	mi
<b>AREA</b>				
cm <sup>2</sup>	square centimeters	0.16	square inches	in <sup>2</sup>
m <sup>2</sup>	square meters	1.2	square yards	yd <sup>2</sup>
km <sup>2</sup>	square kilometers	0.4	square miles	mi <sup>2</sup>
ha	hectares(10,000 m <sup>2</sup> )	2.5	acres	
<b>MASS (WEIGHT)</b>				
g	grams	0.035	ounces	oz
kg	kilograms	2.2	pounds	lb
t	tonnes (1000 kg)	1.1	short tons	
<b>VOLUME</b>				
ml	milliliters	0.03	fluid ounces	fl oz
l	liters	0.125	cups	c
l	liters	2.1	pints	pt
l	liters	1.06	quarts	qt
l	liters	0.26	gallons	gal
m <sup>3</sup>	cubic meters	35	cubic feet	ft <sup>3</sup>
m <sup>3</sup>	cubic meters	1.3	cubic yards	yd <sup>3</sup>
<b>TEMPERATURE (EXACT)</b>				
°C	Celsius temperature	9/5 (then add 32)	Fahrenheit temperature	°F

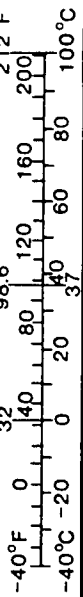


## TABLE OF CONTENTS

	<u>Page</u>
LIST OF ILLUSTRATIONS .....	vii
LIST OF TABLES .....	viii
GLOSSARY .....	ix
EXECUTIVE SUMMARY .....	ES-1
ACKNOWLEDGMENTS .....	ES-11
CHAPTER 1 - INTRODUCTION .....	1-1
1.1 OVERVIEW .....	1-1
1.2 PURPOSE AND REPORT OUTLINE .....	1-2
1.3 CONCEPTS AND TERMINOLOGY .....	1-3
1.4 SUMMARY OF FINDINGS AND RECOMMENDATIONS .....	1-4
1.5 RELATIONSHIP TO OIL SPILL THICKNESS MEASUREMENT .....	1-4
CHAPTER 2 - CONTRAST SIGNATURE PHYSICS .....	2-1
2.1 CONTRAST SIGNATURES .....	2-1
2.2 ATMOSPHERIC TRANSMISSION WINDOWS .....	2-4
2.3 REFLECTIVITY AND EMISSIVITY .....	2-5
2.3.1 Smooth Surfaces: Fresnel Theory .....	2-7
2.3.2 Rough Surface and Volume Scattering .....	2-11
2.3.3 The Assumption of Optical Thickness .....	2-14
2.3.4 Finite Layer Effects .....	2-17
2.4 THERMAL RADIATION: THE PLANCK FUNCTION .....	2-18
2.5 THE LOWTRAN CODE .....	2-22
2.6 OIL AND WATER SURFACE TEMPERATURES .....	2-22
CHAPTER 3 - INFRARED CONTRAST TEMPERATURE CALCULATIONS .....	3-1
3.1 PROCEDURE .....	3-1
3.2 CONTRAST AS FUNCTION OF SEASON AND LATITUDE .....	3-3
3.3 THE EFFECT OF RAIN AND FOG .....	3-6

## TABLE OF CONTENTS (CONTINUED)

	<u>Page</u>
CHAPTER 4 - DATA .....	4-1
4.1    USCG TEST PROGRAM .....	4-1
4.2    IMAGING SENSORS AND CONTRAST TEMPERATURE .....	4-2
4.3    INFRARED IMAGING SENSORS TESTED BY THE USCG .....	4-4
CHAPTER 5 - DATA ANALYSIS AND SENSOR NOISE .....	5-1
5.1    QUALITATIVE CHARACTER OF DATA .....	5-1
5.1.1    Caveats .....	5-1
5.1.2    Qualitative Summary of Nighttime Observations .....	5-1
5.2    IR IMAGERY DATA AND SENSOR SELECTION .....	5-2
5.3    DAYTIME VIDEO AND NIGHT VISION IMAGERY CRITIQUE .....	5-11
CHAPTER 6 - RECOMMENDATIONS .....	6-1
6.1    SENSOR RECOMMENDATIONS .....	6-1
6.2    FURTHER WORK .....	6-1
REFERENCES .....	R-1

Accession For	
NTIS CRA&I	<input checked="" type="checkbox"/>
DTIC TAB	<input type="checkbox"/>
Unannounced	<input type="checkbox"/>
Justification .....	
By .....	
Distribution /	
Availability Codes	
Dist	Avail and/or Special
A-1	

## LIST OF ILLUSTRATIONS

<u>Figure</u>	<u>Page</u>
ES-1 Comparison of Predicted Nighttime Water-Oil Contrast Temperatures for Different Detector Material and for Standard Mid-Latitude Summer Conditions with Sensor Thresholds .....	ES-5
ES-2 The Effect of Season and Latitude on Predicted Nighttime Oil Slick Detectability in 3-5 and 8-12 Micron Bands .....	ES-7
ES-3 Representative LWIR Image of Tank Complex with Test Oil Slicks .....	ES-8
ES-4 MWIR Image of Tank Complex Taken with IRC-160ST on Night of May 5 .....	ES-9
2-1 The Sensing of Contrast Radiance .....	2-2
2-2 The Components of Surface Radiance .....	2-6
2-3 Smooth Surface Reflection and Refraction (Fresnel Theory) .....	2-8
2-4 Emissance of Difference of Oil and Water vs Angle of Observation .....	2-10
2-5 Rough Surface Scatter .....	2-13
2-6 Volume Scatter .....	2-13
2-7 The Spectra of Back-Scattered Light from Two Ocean Surfaces .....	2-15
2-8 The Spectra of the Volume Scattering Coefficient of Two Oils Involved .....	2-16
2-9 Planck Radiation Curves For Temperatures Typical of Standard Environments .....	2-20
2-10 Comparison of the Intensity Components Incident On and Emitted by sea Surface at Standard Conditions .....	2-21
2-11 Characteristic Absorption Lengths of Sea Water and Two Oils .....	2-23
3-1 A Block Diagram of Contrast Temperature Calculation Procedures .....	3-2
3-2 Predicted LWIR Nighttime Water-Oil Contrast Temperatures .....	3-6
3-3 Predicted MWIR Nighttime Water-Oil Contrast Temperatures .....	3-7
3-4 The Effects of Fog and Rain on Predicted LWIR Water-Oil Contrast Temperatures .....	3-8
3-5 The Effects of Fog and Rain on LWIR Atmospheric Path Transmission .....	3-9
4-1 The Relation of Radiometric Contrast Temperature to Measured Contrast Radiance .....	4-5
4-2 The Dependence of Relative Contrast Temperature Sensitivity on Mean Scene Temperature .....	4-6
5-1 Representative Nighttime LWIR Image of Tank Complex .....	5-3
5-2 Representative MWIR Image Tank Complex Taken with IRC-160ST on Night of May 4 .....	5-4
5-3 Representative MWIR Image of Tank Complex Taken with IRC-160 on Night of May 5 .....	5-5
5-4 A Digital Gray Scale Enhancement of a Section of the tank complex seen in Figure 5-2 .....	5-6

## LIST OF ILLUSTRATIONS (CONTINUED)

	<u>Page</u>
5-5 Comparison of Predicted Water-Oil Contrast Temperatures for Night of May 4 with Sensor Thresholds .....	5-7
5-6 Comparison of Predicted Water-Oil Contrast Temperature for Night of May 5 with Sensor Thresholds .....	5-8
5-7 The Effect of Season and Latitude on Predicted Nighttime Detectability in the LWIR and MWIR .....	5-10
5-8 Night Vision Camera Image of Pool Complex .....	5-13
5-9 Relative Contrast Detectable with GEN III Device .....	5-14

## LIST OF TABLES

<u>Table</u>		<u>Page</u>
ES-1 Infrared Imagers .....		ES-2
2-1 Normal Emittance of Oil and Water for Atmospheric Window Regions .....		2-11
4-1 Nighttime Contrast Imagery Data Base .....		4-2
4-2 Infrared Imaging Sensors Tested by USCG .....		4-7
5-1 Measured Environmental Parameters and Standard Summer Atmospheric Values .....		5-2



## GLOSSARY

Absolute Temperature	A temperature scale whose zero is set at $-273^{\circ}\text{C}$ . This temperature is called absolute zero and is the temperature at which all motion and thermal emission cease.
AFGL	Air Force Geophysics Laboratory, at Hanscom Field, Bedford Mass. Developer of standard atmospheric models.
EC	Environment Canada.
FLIR	Forward-looking Infrared. A sensor which detects the thermal radiation from a scene and converts this thermal image to a TV image for visual assessment. Usually, the term refers to a gimbal-mounted sensor, but sometimes, as in this test, also includes hand-held devices.
Fresnel Theory	The theory which allows the incident angle-dependent reflectivity of an ideally smooth surface from knowledge of the bulk refractive index of the surface material.
Gen III	The current state-of-the-art image intensifier night vision (third generation) sensor technology.
HgCdTe	Mercury-Cadmium-Telluride, a detector material commonly used for LWIR sensors.
InSb	Indium-Antimonide, a detector material for sensing out to 5 microns.
Kelvin Temperature	See Absolute Temperature.
Lambertian Scatter	Isotropic scatter from an ideally rough surface.
LOWTRAN-7	A computer code, developed by the Air Force Geophysics Laboratory for calculating the absorption and thermal emission of atmospheres for arbitrary meteorological conditions.

## GLOSSARY (Cont'd)

LWIR	Long-Wavelength Infrared, the spectral region between 8 and 12 microns. This is an atmospheric transmission window and a region in which the earth, ocean, and atmosphere emit thermal infrared radiation strongly (see MWIR).
MWIR	Mid-Wavelength Infrared, the spectral region between 3 and 5 microns. This is an atmospheric transmission window and a region in which the earth, ocean, and atmosphere emit routinely measurable thermal infrared radiation (see LWIR).
PbSe	Lead Selenide, a detector material used for sensing in the infrared out to 5 microns.
Planck Function	A function describing the spectral distribution of thermal energy radiated by a perfect emitter (a black body). The distribution is a function of wavelength, $\lambda$ , and absolute temperature, T.
PtSi	Platinum Silicide, a detector material used for sensing in the visible and infrared out to 4-5 microns.

## **EXECUTIVE SUMMARY**

### **Background**

The detection of oil slicks on the ocean's surface is an operational requirement of the U.S. Coast Guard's Marine Environmental Protection mission. In clear weather, daytime detection of a slick that is sufficiently thick to justify the deployment of cleanup resources is usually routine. Such a slick is easily detectable by direct visual inspection or with the aid of video or infrared imagers. The eye visually senses reflected sunlight in the 0.4 - 0.7-micron spectral region. Thermal infrared radiation from a typical scene becomes routinely detectable at wavelengths of 3 microns and longer.

Nighttime detection is much more difficult. Natural illumination levels (even from a full moon) are not adequate for reliable direct visual detection. Fortunately, commercially-available sensors operating in the 8 - 12-micron spectral region are capable of detecting the small differences in radiation at night, from oil and water. Slick detection at night can currently be done by the Coast Guard using airborne, gimbal-mounted thermal imagers which operate in this spectral region. These infrared sensors detect thermal images of the scene, that is, images of the heat radiated (rather than light scattered) by various features of the scene, and convert them to images on a television screen for viewing and interpretation.

The 8 - 12-micron and 3 - 5-micron wavelength bands are two infrared spectral regions where the atmosphere does not strongly absorb, thus enabling the thermal imaging of oil slicks. The 8 - 12-micron region is called the long-wave infrared (LWIR) and the 3 - 5-micron region is called the medium wave infrared (MWIR). The gimbal-mounting of existing Coast Guard LWIR imagers increases their cost and limits their data-taking capability to specific aircraft. Hand-held imagers which operate in the MWIR are now

commercially-available at relatively low cost. These sensors offer the advantages of portability and platform independence on a level similar to television cameras.

The primary goal of this study is to compare the predicted oil slick detection performance of sensors operating in the two infrared bands and to validate the predictions with a limited set of field test data. These analyses will provide a basis for determining whether commercially-available, portable thermal imagers offer a reliable nighttime oil slick detection capability. A secondary objective is to assess whether commercially-available, visible-spectrum night vision systems (low-light level TVs) are capable of detecting oil slicks at night.

### Sensors

Three hand-held MWIR imagers were obtained from commercial vendors for the field evaluation. These sensors differ somewhat in cost and capability. Although cost is not considered here, it should be addressed in any final comparison of sensors' mission value. Table 1 lists these sensors and their pertinent attributes together with data on the two Coast Guard gimbal-mounted LWIR systems tested. Thus, the initial field comparison of hand-held to gimbal-mounted sensors, reported on here and in greater detail in a companion report, became a comparison of MWIR and LWIR performance as well.

**TABLE ES-1**  
**Infrared Imagers**

<b>IMAGER</b>	<b>IR BAND MICRONS</b>	<b>DETECTOR TYPE</b>	<b>ADVERTISED SENSITIVITY (°K)</b>
FLIR 2000	8 - 12	Hg Cd Te	0.2
WF-360TL	8 - 12	Hg Cd Te	0.1
IRC-160ST	3 - 5	InSb	0.04 @ 27°C
Thermovision	3 - 5	Pb Se	0.1 @ 30°C
FSI PRISM	3 - 5	PtSi	0.2 @ 30°C

## **Approach**

This assessment of the relative utility of MWIR and LWIR imagers is primarily theoretical, with field data used for semi-quantitative confirmation of theoretical conclusions. The theoretical analysis is based upon the Fresnel Theory of reflection and the Planck Theory of thermal radiation. The Fresnel Theory allows one to calculate the emissive or reflective properties of a surface given the wavelength dependent, bulk refractive index of the surface material (e.g., oil or water). The Planck Theory allows one to calculate, given a surface emissivity, the thermal radiation from a surface in various sensor bands (e.g., MWIR or LWIR) given the surface temperature - a meteorological condition. The driving factor separating (slightly) the thermal signature of oil from water at night is the difference in refractive index of oil from water. This difference, through the Fresnel Theory, determines a surface emissivity difference and so a difference in the thermal radiation from an oil slick and water. In the terminology of radiometry one says that oil and water have different "radiometric temperatures" or a "contrast temperature" difference.

A set of field data is available for use in semi-quantitative confirmation of theory. The U.S. Coast Guard was invited to participate in an Environment Canada-sponsored field measurement program in May 1993 at Petawawa, Ontario. A complex of twelve shallow, water-filled, rectangular test pools was built in a 480 ft long by 100 ft wide test bed. In nine of these twelve pools various oil types were spilled in controlled amounts; the other three contained only water. The sensors of Table 1 were flown on fixed-wing aircraft and helicopters, making several passes over the tanks on two successive nights, May 4 and May 5, 1993. The imagery was recorded on analog tape and converted to digital form at the Coast Guard Research and Development Center. The data were not calibrated and so allowed only a semi-quantitative confirmation (i.e., in terms of detection thresholds) of theoretical results. Meteorological data (temperature and humidity) were available as inputs to theoretical calculations specific to the measurement conditions. Image data on the pool complex were also taken with a night vision camera system, a state-of-the-art low light level TV. The night vision camera data, on analysis, were set

aside as not relevant to the question of the detection of oil slicks on water. The reason was that the water in the tanks was only 6 inches deep. Consequently, one saw water surface images dominated by the strong reflection of light from the bottoms of the tanks and not by the weak reflection from the oil and water surfaces.

### **Theoretical Analysis**

The results of the theoretical analysis will be discussed first and then related to the data acquired in the Canadian field measurement program. In the theoretical work, the nighttime radiances from an oil slick and from a water surface are calculated, for various environmental conditions (e.g., temperature, humidity) including conditions specific to the field experiment data. The differences between the oil and water radiances are expressed (as is conventional) in terms of a "radiometric temperature" difference. That is, the slight difference in radiance is assumed to be equal to a difference between two ideal emitters (i.e., black bodies) with slightly different temperatures. The resulting temperature difference is conventionally called the "contrast temperature difference." It is important to note that all theoretical calculations made in this report assume that the oil and water are at the same physical temperature; that is, a worst-case scenario in which the oil and water have reached equal temperature is assumed. This physical temperature assumption is not to be confused with the term "radiometric temperature" used above.

Theory, as developed here, predicts that water should appear radiometrically about 1°C warmer than oil during the night in LWIR (8 - 12 microns) and about 0.1°C warmer than oil in the MWIR (3 - 5 microns). These differences, as stated above, are the results of differences in the refractive indices of oil and water and so surface emissivities. These indices are wavelength dependent and the results are graphically summarized in Figure ES-1 in which predictions of apparent temperature difference, as measured by an airborne sensor at 500 ft altitude, are plotted versus sensor viewing (incidence) angle  $\theta$ . The environmental conditions assumed in the calculation are those of a standard

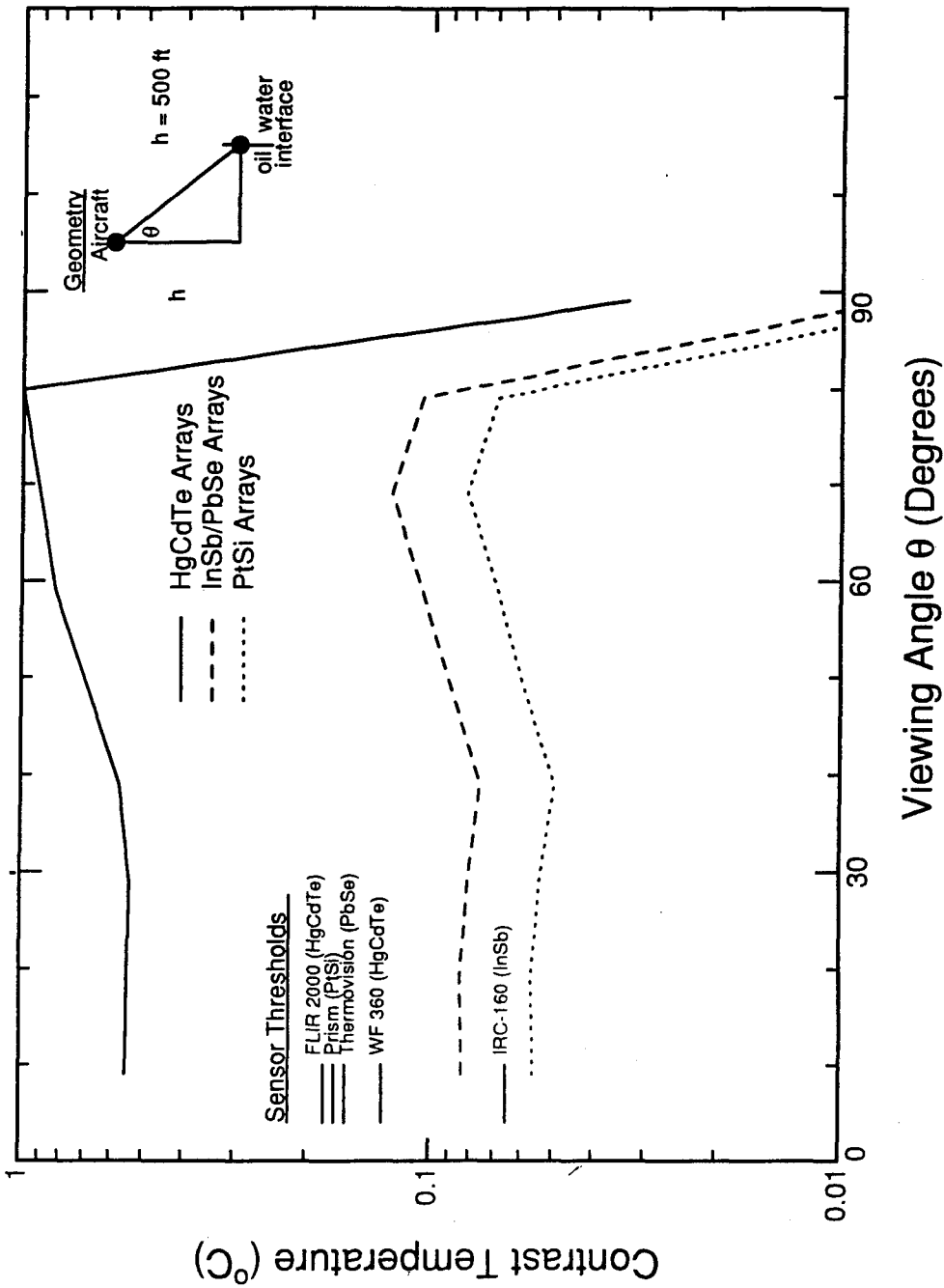


Figure ES-1. Comparison of predicted nighttime water-oil contrast temperatures for different detector material and for standard mid-latitude summer conditions with sensor thresholds. Sensor threshold (horizontal line segments) must fall below calculated contrast for specific material for oil to be detectable.

mid-latitude summer atmosphere which corresponds to a sort of mean condition for the nights of May 4 and May 5, 1993 during which the data were taken. The sensor sensitivities from Table 1 (slightly adjusted for temperature) are indicated by horizontal bars in Figure ES-1. The predicted LWIR contrast temperatures exceed the LWIR imagers' sensitivities in Figure ES-1, and thus should be detectable. The sensitivities for the Thermovision 210 and FSI Prism fall above the MWIR oil-water contrast predictions as shown. Thus the theoretical analysis indicates that these sensors are not sufficiently sensitive to detect nighttime oil-water contrast. The IRC-160 ST sensitivity falls almost on the predicted contrast curve and so oil-water contrast with this detector should be marginal. The calculations were repeated for various sets of standard atmospheric conditions representing latitudinal and seasonal variations. The results are summarized in Figure ES-2. In all cases the LWIR contrast is moderately above the LWIR sensor thresholds and the predicted MWIR contrast is very near the contrast temperature sensitivity of the IRC-160 ST, the most sensitive of the MWIR imagers.

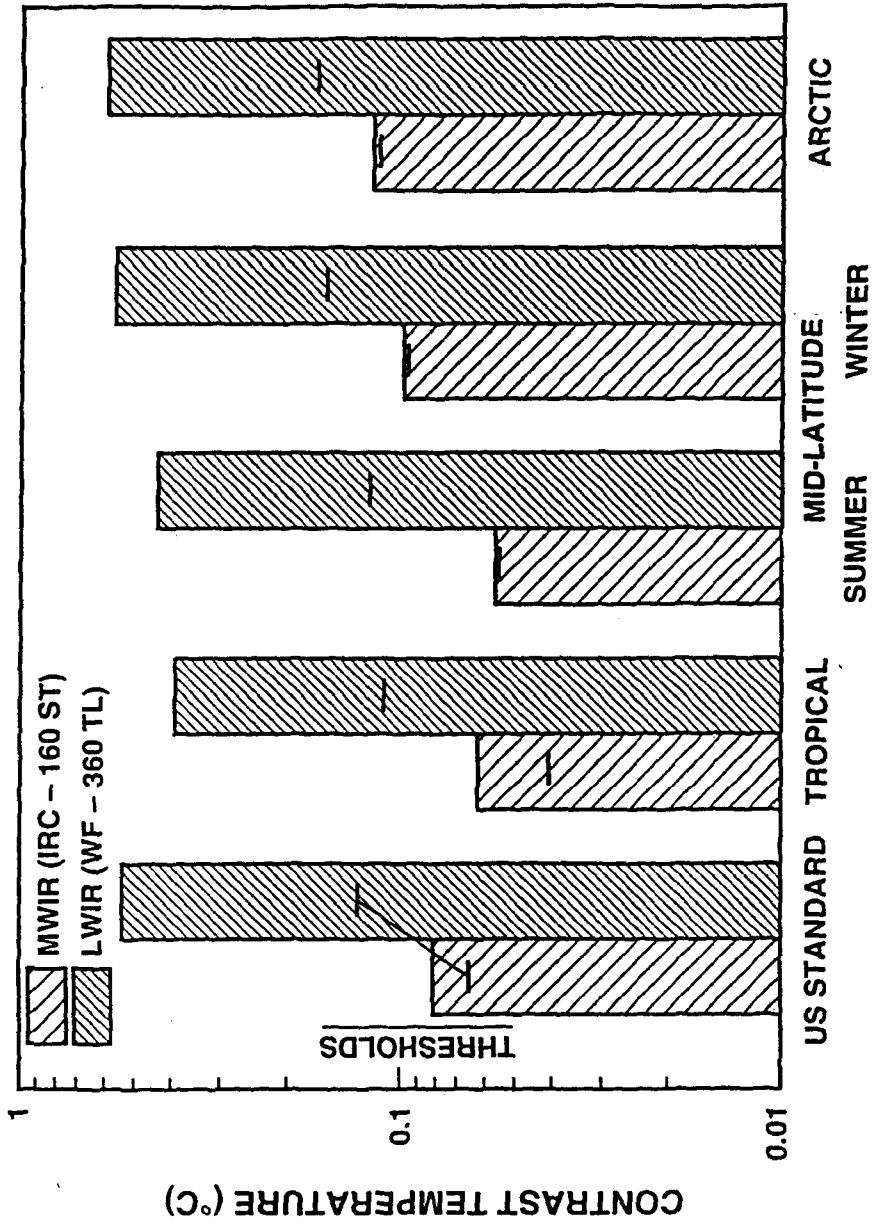
### **Image Analysis**

Figures ES-3 and ES-4 are samples of WF-360TL LWIR imaging data and IRC-160 ST MWIR imaging data from the night of May 5. These images semi-quantitatively confirm the theory-based statements just made. LWIR contrast is clear and MWIR contrast, with the most sensitive imager of Table 1, is marginal. MWIR contrast as obtained with the IRC-160 ST on the night of May 4 was lower than that of Figure ES-4 and at best, questionably detectable with digital contrast enhancement.

### **Conclusion**

Theory and data indicate that existing U.S. Coast Guard and other commercially available LWIR infrared imagers should reliably detect oil slicks on water at night. The detection of such slicks even with quite sensitive, commercially available MWIR imagers is





AFGL STANDARD ATMOSPHERES

Figure ES-2. The effect of season and latitude on predicted nighttime oil slick detectability in 3-5 and 8-12 micron bands. Sensor thresholds (horizontal line segments) are all below calculated contrasts (vertical bars) so oil is always detectable, though marginally for the MWIR.

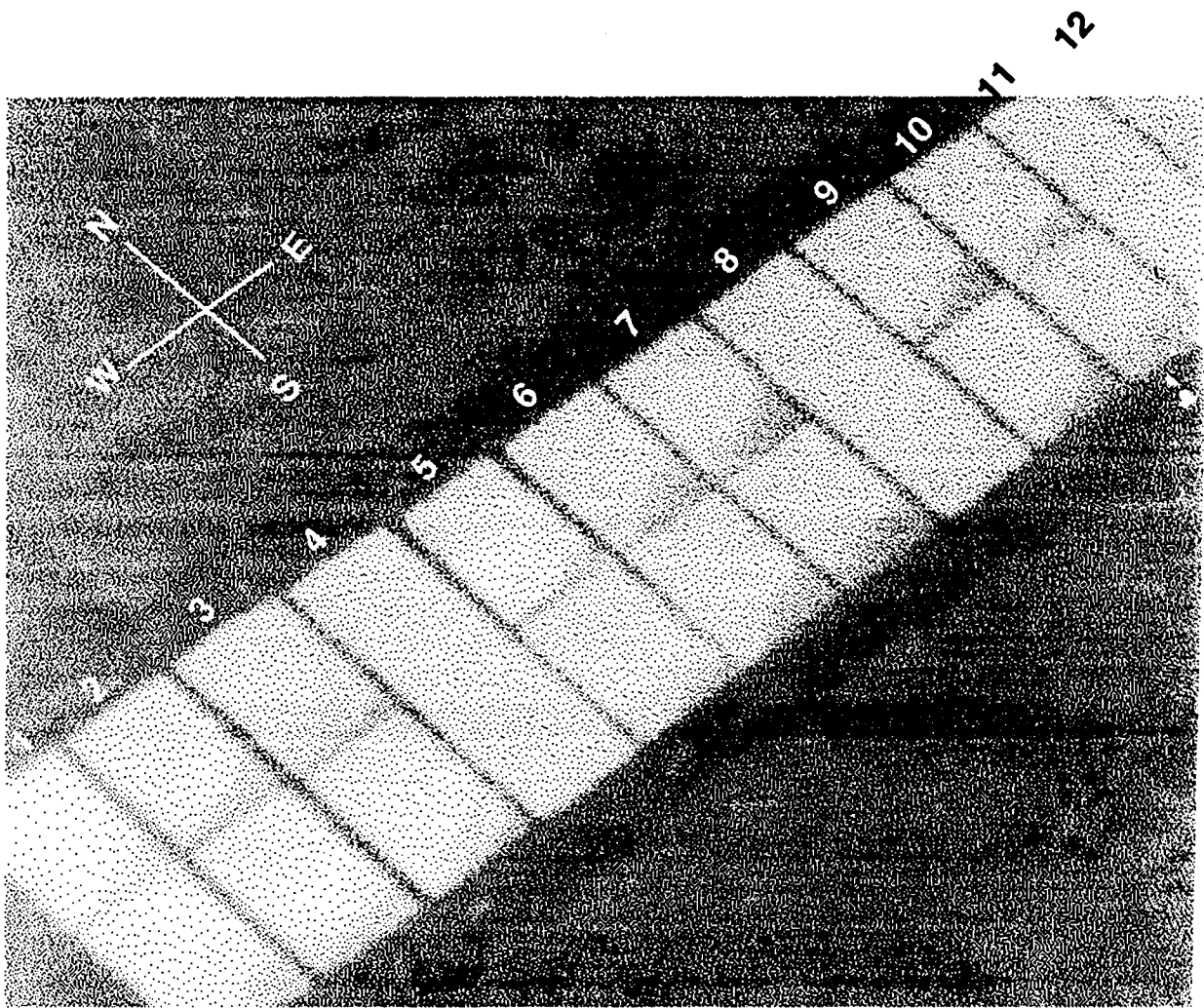


Figure ES-3. Representative LWIR image of tank complex with test oil slicks.

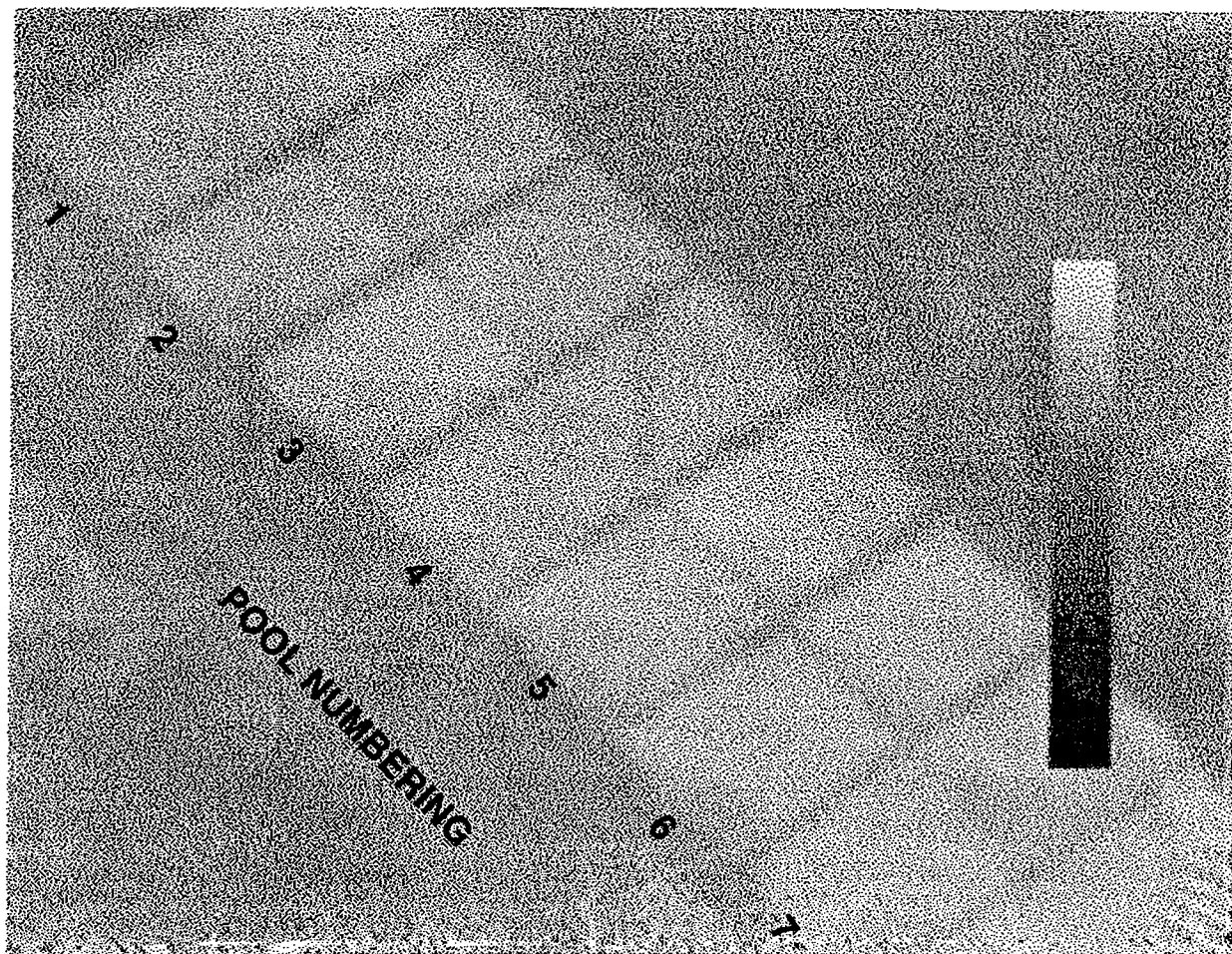


Figure ES-4. MWIR image of tank complex taken with IRC-160ST on night of May 5.

marginal. However, since the most capable of the tested MWIR imagers, the IRC-160 ST, is in fact more sensitive than the LWIR imagers of Table 1, it could prove a more useful instrument for imaging the detailed structure of scenes with sufficient radiometric temperature contrast (e.g., - solar-heated surfaces during the day). Such MWIR imagers should readily detect oil-water contrast when even small ( $<1^{\circ}\text{C}$ ) physical temperature differences exist, and are expected to perform best in warm environments (see Figure ES-2).

### **Recommendations**

The LWIR (8 - 12 micron) band is preferred over the MWIR (3 - 5 micron) band for the detection of oil slicks at night. This recommendation is based upon theoretical analysis and is physically based upon the fact that the difference in emissivities between oil and water is significantly larger in the LWIR than in the MWIR. Semi-quantitative experimental data taken during two sets of night flights in which three MWIR and two LWIR infrared imagers were exercised against documented oil-water targets lend further support to this recommendation.

The value of low-noise, sensitive imagers operating in the visible and near-infrared (e.g., night vision cameras) has not been fully explored. Devices are now coming into operation which are low-light level CCD cameras with very low noise factors. This potential for nighttime oil slick detection should be studied theoretically first, then experimentally.

A set of calibrated field measurements of oil slicks on water should be made with a set of representative, state-of-the-art, commercially available MWIR and LWIR imagers.

## **ACKNOWLEDGMENTS**

Our thanks to J.V. Plourde of Analysis and Technology, Inc., New London Connecticut for his work in data reduction and analysis. We also wish to thank the following MIT Lincoln Laboratory personnel: Mrs. Dea Cincotta and Miss Andrea Carlton for their support in programming and Ms Paula Jones for her patience and industry in report preparation.

# CHAPTER 1

## INTRODUCTION

### 1.1 OVERVIEW

This effort is directed to determining the appropriate choice of sensors for detecting oil spills at night from low-flying aircraft. This report is specifically concerned with infrared (heat-detecting) imaging sensors and, in passing, with night-vision (low-light level TVs) imaging sensors. Both types of sensors present to the user an image of the oil spill (or oil slick) on water, and this output is "matched" in contrast levels, scan rate, and wavelength band to the visual response characteristics of the human eye. The user interprets the image based upon his or her experience and makes a judgment upon the probability and character of an oil spill. The "match" to visual response characteristics is made for infrared sensors by converting the sensed thermal radiation, at wavelengths from 3 - 5 or 8 - 12 microns, to visible radiation at 0.4 - 0.7 microns on a TV-like screen. The "match" for night vision sensors is made by sensing the low, nighttime light levels with photo-sensitive, current generating devices, amplifying these currents, and reconverting these electron currents to TV imagery.

During the day oil spills are usually easily detectable by eye and with thermal infrared (IR) imagers or forward-looking infrared sensors (FLIRs). These designations, IR imager and FLIR, will be used interchangeably in this text. The spills are detectable by eye because oil usually presents a sufficient intensity contrast (a few percent) and color contrast with water for visual detection. Oil spills are detectable by thermal sensors because oil is heated by sunlight (because of its strong absorption of visible wavelengths) a few degrees above adjacent water surfaces. Such temperature differences are easily detectable by commercially available FLIRs.

At night the situation is quite different and spill detection is more difficult. In the visible the eye's contrast sensitivity is poor (~10%) at low nighttime illumination levels, while oil-water contrast is low (1-2%). Quite sensitive night-vision sensors are required to detect such differences. In the infrared, since oil and water are at essentially the same temperature, the oil-water contrast depends upon the small differences in emissivity (~1 -2%) between oil and water. Infrared contrast detection thus requires sensitive FLIRs and such devices are commercially available.

## **1.2 PURPOSE AND REPORT OUTLINE**

In this report, the physics supporting the above statements will be developed and the statements on nighttime detection supported by calculations. The choice of preferred nighttime sensor will be explored in the framework of this physics. An infrared image data set gathered by the U.S. Coast Guard during a May 1993 experiment in Ontario, Canada [reference 1] will be related to this phenomenology analysis. Several optical/IR sensors and a variety of documented, oil-on-water scenes are represented in the image data. Sensor recommendations will be made based on this analysis.

Beyond the just-stated purposes of justifying sensor recommendations, this report is written to familiarize the reader with the physics of IR contrast signature generation and detection. Section 2, reviewing contrast signature phenomenology and physics, and Section 3, on contrast (i.e., oil-water) calculations, are directed towards that end. The reader, familiar with such fundamental matters, may proceed directly to Section 4 where the data gathering program mentioned above, which is directly relevant to the goal, (i.e., FLIR sensor choice) is described. Selected data obtained on this program, primarily at night, are analyzed in Section 5 using the principles and theory outlined in Sections 2 and 3. The results of this work are summarized in Section 6 as recommendations of sensor choice for nighttime spill detection and for further measurement work.

### 1.3 CONCEPTS AND TERMINOLOGY

This analysis makes use of a half-dozen concepts from thermal physics. They are discussed in the body of the text, but summarized briefly here as a framework for the recommendations of the next subsection. The concepts are: thermal or heat radiation, thermal imaging sensors, thermal contrast detection, thermal emittance, the Fresnel Theory of emittance and reflectance, and finally, the thermal absorption and emissions of the atmosphere.

All bodies at temperatures above absolute zero ( $0^{\circ}\text{K}$ , or  $-273^{\circ}\text{C}$ ) radiate electromagnetic energy or thermal radiation. The spectrum of this thermal radiation for a given body temperature will peak at a specific wavelength. The spectrum of the sun, a body at about  $6000^{\circ}\text{K}$ , peaks at about 0.5 micron wavelength (in the visible spectrum), while bodies at room temperature,  $300^{\circ}\text{K}$ , have a spectrum peaking at about 10 microns (in the infrared). During the day and night objects can be "seen" with sensors that detect their infrared heat radiation. These are thermal sensors.

Thermal imaging sensors convert the infrared radiation from a body at room temperature into an image which can be seen by the eye, on a TV-like, phosphor screen. Objects are detected (in both the infrared and in reflected sunlight) by the contrast in radiation from a body and its background, or immediate vicinity. The thermal radiation from a body is determined by the body's temperature, the wavelength at which the radiation is sensed, and a parameter,  $\epsilon$ , called the emittance, ( $0 < \epsilon < 1$ ). The emittance of a surface and the reflectance,  $r$ , of a surface together sum to unity ( $\epsilon + r = 1$ ). The emittance of a smooth surface depends only upon the refractive index,  $n$ , of the material of the surface and upon the observing angle. The theory which gives this emittance is called Fresnel Theory. The clear atmosphere absorbs and emits infrared radiation. The theory and physics governing this thermal behavior is quite complex but has been implemented by the Air Force Geophysical Laboratory in a computer code called LOWTRAN. This code can be used



to calculate atmospheric absorption and emission at all wavelengths, observing geometries, and meteorological conditions of interest.

#### **1.4 SUMMARY OF FINDINGS AND RECOMMENDATIONS**

While more detailed recommendations are given in Section 6, the major points are given here. First, FLIRs operating in the LWIR (long wavelength infrared, 8 - 12 microns) band are preferred over MWIR (mid wavelength infrared, 3 - 5 microns) FLIRs for nighttime imaging of oil spills from airborne platforms. Such LWIR sensors are in fact currently operational on Coast Guard aircraft. Advanced MWIR imagers also have some capability of nighttime spill detection, but this capability will be stressed by some oil types and environmental conditions. Second, considering the advances in low-noise, high sensitivity silicon arrays (CCD) for nighttime imagers (low-light level TVs), a short study assessing the potential of such devices for spill detection is warranted. Third, further night IR imaging data on oil spills is desirable, both in the uncontrolled conditions of a real spill, and under controlled conditions with sensor calibration targets in the scenes to validate data-theory comparisons. Finally, when sufficient radiometric contrast exists, (as is the case during the day) state-of-the art MWIR imaging sensors may be preferred over currently-operational LWIR imagers. The technology level for making larger detector arrays is more advanced in the MWIR than LWIR. The resulting superior contrast sensitivity should allow greater discrimination of detail in MWIR rather than LWIR oil slick imagery.

#### **1.5 RELATIONSHIP TO OIL SPILL THICKNESS MEASUREMENT**

This report is concerned with the detection of an oil spill or slick at night. The actual thickness of the spill (other than it be sufficient for the analysis of this report to be applicable) is not of concern. To direct a spill clean-up, however, the measurement of the thickness of various areas of the spill is of great concern. Several procedures have been suggested for such thickness measurements over the years. A companion volume

to this report describes work on a technique called "Frequency Scanning Radiometry" for effecting such measurements [reference 2]. The concept originated at MIT Lincoln Laboratory, and its hardware realization was developed at MIT Lincoln Laboratory under Coast Guard funding. The technique has been shown to be capable of measuring, under laboratory conditions, slick thickness of about 0.5 millimeter and greater.

## CHAPTER 2

### CONTRAST SIGNATURE PHYSICS

#### 2.1 CONTRAST SIGNATURES

An object is "seen" by a sensor by the difference or contrast in radiation reaching the sensor from the object and its immediate vicinity or "background." The radiation from the body and its background can be reflected radiation originating from some other source (such as sunlight) or radiation emitted from the body itself. Self-emitted radiation is often termed "thermal radiation."

Natural sources of reflected radiation at earth's surface include the sun, the moon, and the faint airglow of the night sky, which all are predominately at wavelengths ranging from the ultraviolet (0.3 microns) to the near-infrared (< 3 microns), and thermal radiation from the atmosphere at wavelengths longer than 3 microns. The predominant natural source of radiation emitted by bodies on earth's surface is thermal, or Planck, radiation which is discussed in Section 2.4. This radiation dominates contrast signatures at wavelengths in the mid-infrared and longer (> 3 microns).

Consider the observation sketched in Figure 2-1. Let  $J_o(\Delta \lambda)$  be the radiance in (watts/cm<sup>2</sup> - Steradian) due to reflection or emission emanating from the surface of an object in a wavelength band:  $\Delta \lambda$ , and  $J_b(\Delta \lambda)$  be the radiance from the adjacent background. Then the object-background contrast radiance,  $C(\Delta \lambda)$ , seen by a sensor operating in the passband  $\Delta \lambda$  is

$$C(\Delta \lambda) = \tau(R, \Delta \lambda) [J_o(\Delta \lambda) - J_b(\Delta \lambda)] \quad (2-1)$$

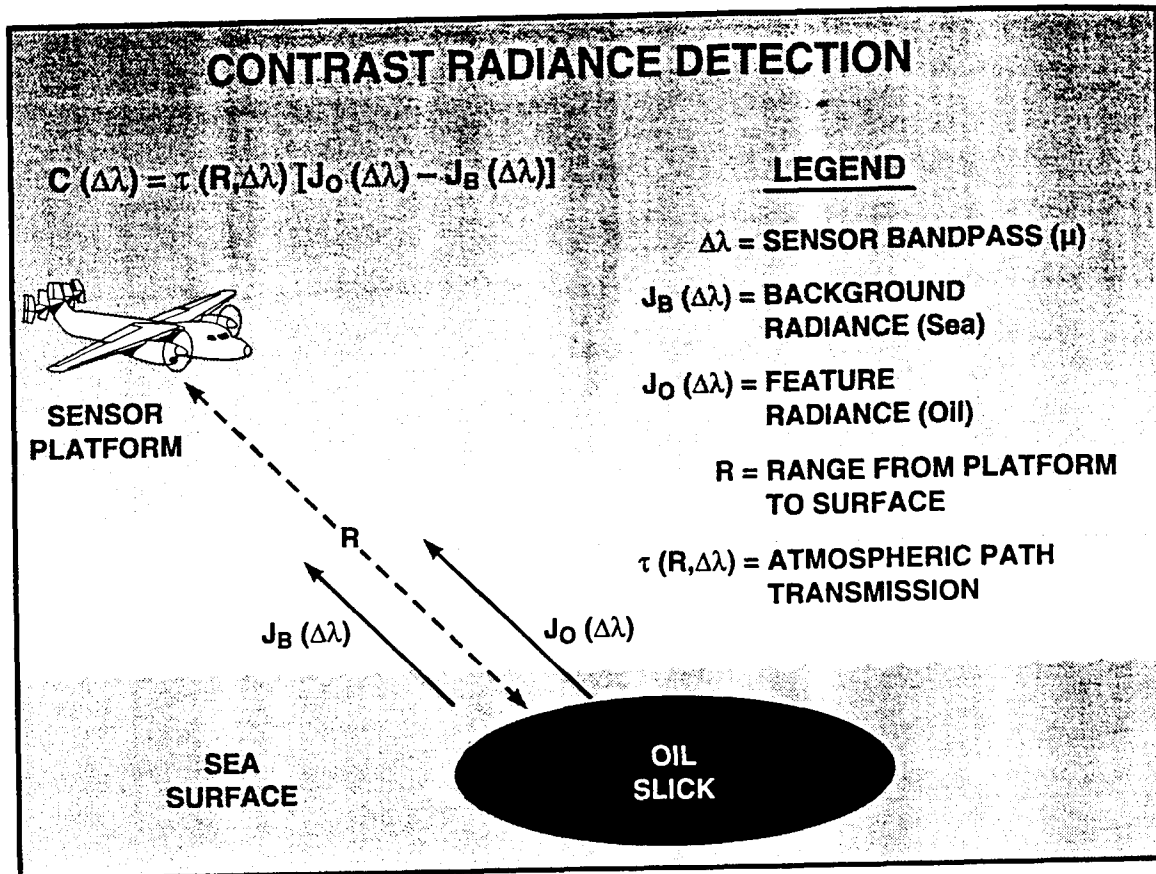


Figure 2-1. The sensing of contrast radiance. A sensor at range,  $r$ , operating in bandpass,  $\delta\lambda$ , measures the radiance difference between a surface feature,  $j_o(\delta\lambda)$ , and its background surface radiance,  $j_b(\delta\lambda)$ .

where  $\tau(R, \Delta\lambda)$  is the transmission of the atmospheric path of range  $R$  from object to sensor. If this contrast is greater than some threshold level:  $C_o(\Delta\lambda)$ , depending upon the specific sensor used in the observation, the contrast is detected. Equation (2-1) adequately represents the measurement situation for most thermal infrared sensors, particularly the ones of concern here. The modeling compressed into Equation (2-1) requires some extension for night vision sensors where  $C_o(\Delta\lambda)$ , the sensor contrast threshold depends on the absolute radiance levels,  $J_o(\Delta\lambda)$  and  $J_B(\Delta\lambda)$ , as well as their difference. There is also a dependence on the angular size of the object. These matters are treated briefly in Section 4.2 where the imaging sensors are discussed.

Finally, for some sensors at high radiance levels, such as ordinary daytime viewing with the eye, it is often more appropriate to analyze contrast detection in terms of "relative" contrast:  $\Delta C(\Delta\lambda)$ , where

$$\Delta C(\Delta\lambda) = \frac{C(\Delta\lambda)}{J_B(\Delta\lambda)} \quad (2-2)$$

Relative contrast is the fractional, or percentage difference in radiance from a feature and its background (e.g., an oil slick on water). It is thus the difference in radiance between an object and its background divided by the background radiance. The eye can usually detect relative contrast levels of 2 - 3% during the day. At night the eye is much more sensitive in the absolute sense, that is to  $C(\Delta\lambda)$ , but less sensitive in the relative,  $\Delta C(\Delta\lambda)$ , sense. Thus, oil-water contrasts which can be seen in sunlight might not be seen in moonlight.

To analyze contrast detection we need theory or data that give us:  $J_o(\Delta\lambda)$ ,  $J_B(\Delta\lambda)$ , and  $\tau(\Delta\lambda)$ , which are all determined by "nature" as discussed below, and  $C_o(\Delta\lambda)$ , which depends on the characteristics of a given sensor.

## 2.2 ATMOSPHERIC TRANSMISSION WINDOWS

Remote sensing of oil spills can be and has been done at: ultraviolet, visible, infrared, millimeter and microwave wavelengths [references 3 - 8]. This report on nighttime detection is concerned primarily with infrared, that is thermal, radiation, and secondarily with detection at visible and near IR wavelengths (0.4 - 1.0 microns) region. As stated earlier, passive oil spill detection and thickness measurement at millimeter waves, with some reference to microwaves, is treated in a companion report [reference 2].

The atmosphere, of course, transmits fairly well in the visible, (0.4 - 0.7 microns), though this transmission is highly variable (due to haze and fog). The nominal standard path length at which an object can be detected at earth's surface is 23 km, a distance primarily determined by typical atmospheric aerosol or dust levels. For a given path, however, actual path transmission can vary from a few kilometers in haze, or tens of meters in fog, to more than 50 km for particularly clear, dust free days. Outside the visible band it is the atmospheric molecules themselves, rather than atmospheric dust, which dominate absorption and so determine path transmission:  $\tau(\Delta\lambda)$ . While the major atmospheric gases (nitrogen and oxygen) do not (with trivial qualifications) absorb in the near-ultraviolet, visible, and infrared, the minor atmospheric gases (water vapor, carbon dioxide and ozone) absorb strongly in wavelength regions or "bands" specific to each molecule. Ozone absorbs radiation with wavelengths shorter than 0.3 microns while carbon dioxide, ozone, and water absorb strongly in various bands within the infrared, [reference 9].

The effect of these absorptions is to limit thermal infrared sensors (at least in the lower atmosphere) to atmospheric transmission "windows," specifically at: 3.0 - 4.0, 4.5 - 5.0, and 8.0 - 12.0 microns. The data analyzed in Section 5 were taken with sensors operating in these wavelength regions. There are other "windows" in the 1.0-3.0 micron region but they are not pertinent to this effort. The wavelength region from 3.0-5.0 microns is referred to as the MWIR (mid-wavelength infrared), while the region from 8.0-

12.0 microns is called the LWIR (long-wavelength infrared). The data acquired for this effort include imagery in both the MWIR and LWIR.

### 2.3 REFLECTIVITY AND EMISSIVITY

In the discussion of Equation (2-1) it was noted that the radiance of a body or background will be the result of reflected or/and emitted radiation. The situation is schematically indicated in Figure 2-2. Symbolically then

$$J(\Delta\lambda, \theta) = r(\Delta\lambda, \theta)I(\Delta\lambda, \theta) + \epsilon(\Delta\lambda, \theta) P(\Delta\lambda, T_s) \quad (2-3)$$

where the first term on the right of Equation (2-3) is reflected radiation and the second term is emitted increases toward horizon,  $\theta=90^\circ$  radiance.  $J(\Delta\lambda)$  can be either object,  $J_o$ , or background,  $J_b$ , radiance and is expressed in units of watt/cm<sup>2</sup>- steradian and

- $r(\Delta\lambda, \theta)$  = the "reflectivity," or reflectance, of the surface in bandpass,  $\Delta\lambda$ , at incident angle  $\theta$
- $I(\Delta\lambda, \theta)$  = the intensity of radiation incident on the surface in bandpass,  $\Delta\lambda$ , at incident angle  $\theta$ . In the infrared this will primarily be from atmospheric thermal radiation, the solar component is usually negligible.
- $\epsilon(\Delta\lambda, \theta) =$  the "emissivity," or reflectance, of the surface in  $\Delta\lambda$  bandpass at incident angle  $\theta$
- $P(\Delta\lambda, T_s) =$  the thermal or Planck, black-body emission from the surface at temperature  $T_s$  in bandpass  $\Delta\lambda$

Equation (2-3) is "notional" in the sense that it condenses a rather complex phenomenology into a simplified form for convenience of discussion. Reflectivity,  $r(\Delta\lambda, \theta)$  and emissivity,  $\epsilon(\Delta\lambda, \theta)$ , are considered here, while  $I(\Delta\lambda, 58,17)$  and  $P(\Delta\lambda, T_s)$  are treated later in Section 2.4.

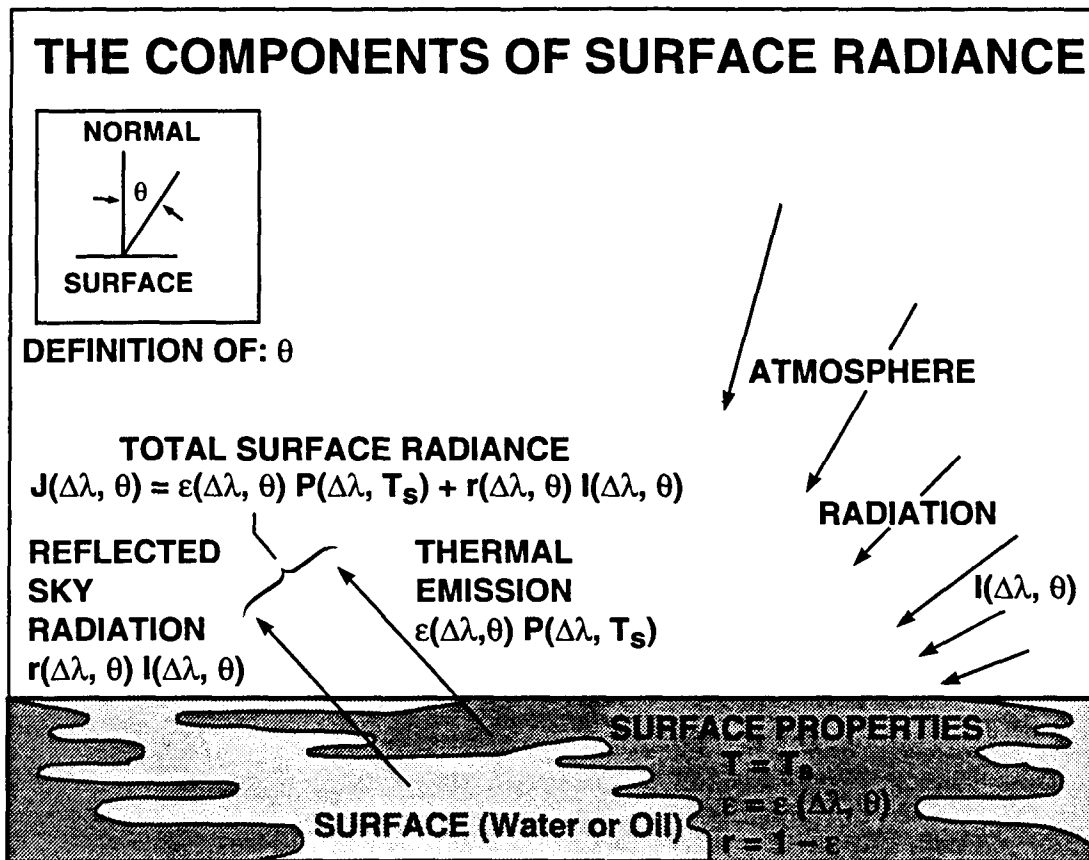


Figure 2-2. The components of surface radiance. Surface radiance depends upon bandpass,  $\delta\lambda$ , and angle of incidence  $\theta$ . It is a mixture of thermally-emitted surface radiation,  $\epsilon p$ , and reflected atmospheric radiation,  $r_i$ . Atmospheric radiation intensity increases toward horizon,  $\theta = 90^\circ$ .



For most surfaces, including the oil and water of this analysis, reflectivity and emissivity are complementary, that is:

$$e(\Delta\lambda, \theta) = 1 - r(\Delta\lambda, \theta) \quad (2-4)$$

so a theoretical discussion of reflectance includes the physics of emittance. Surface reflectance is often discussed and analyzed in terms of its two limiting cases: reflections from "smooth surfaces," or Fresnel reflection, and reflection from perfectly "rough" or Lambertian surfaces. The terms "smooth" and "rough" refer to the variation of surface properties of the reflecting surface over scales of-the-order-of the wavelength of radiation of concern. If this variation is considerable the surface is rough; if negligible the surface is smooth. This analysis is concerned with oil and water surfaces that are both smooth and flat. The surface of even a rough sea can thus be taken as flat (though tilted) for the purposes of this analysis. A smooth, shaped surface, such as a water drop, can act as an optical element (a lens) but such behavior is not relevant to this discussion.

### **2.3.1 Smooth Surfaces: Fresnel Theory**

The reflectance, and emittance, of a smooth, flat surface is described by Fresnel theory as summarized here and in [reference 10]. The theory is adequate for the ocean surface for a wide range of conditions. The surface reflectance (in air) in this theory is determined by:  $\Delta\lambda$ , the bandpass of sensor concern;  $\theta$ , the angle of incidence of radiation incident on (or emitted by) the surface; and  $n(\Delta\lambda)$ , the bulk refractive index of the reflecting medium. Figure 2-3 represents the process discussed here. Fresnel Theory can be summarized in three equations: the first relating the easily-measured reflectance of a surface of normal incidence,  $r_o(\Delta\lambda)$ , to the refractive index of the reflecting medium,  $n(\Delta\lambda)$ ; the second relating the angle relative to normal,  $\theta_r$ , of a refracted ray in the medium (water or oil) for a ray incident on the surface (from air) at an angle,  $\theta_i$ ; and the third giving reflection coefficient,  $r(\Delta\lambda, \theta)$ , of the beam reflected back into air at the specular angle:  $-\theta_i$ . The situation is represented in Figure 2-3 and the specific equations

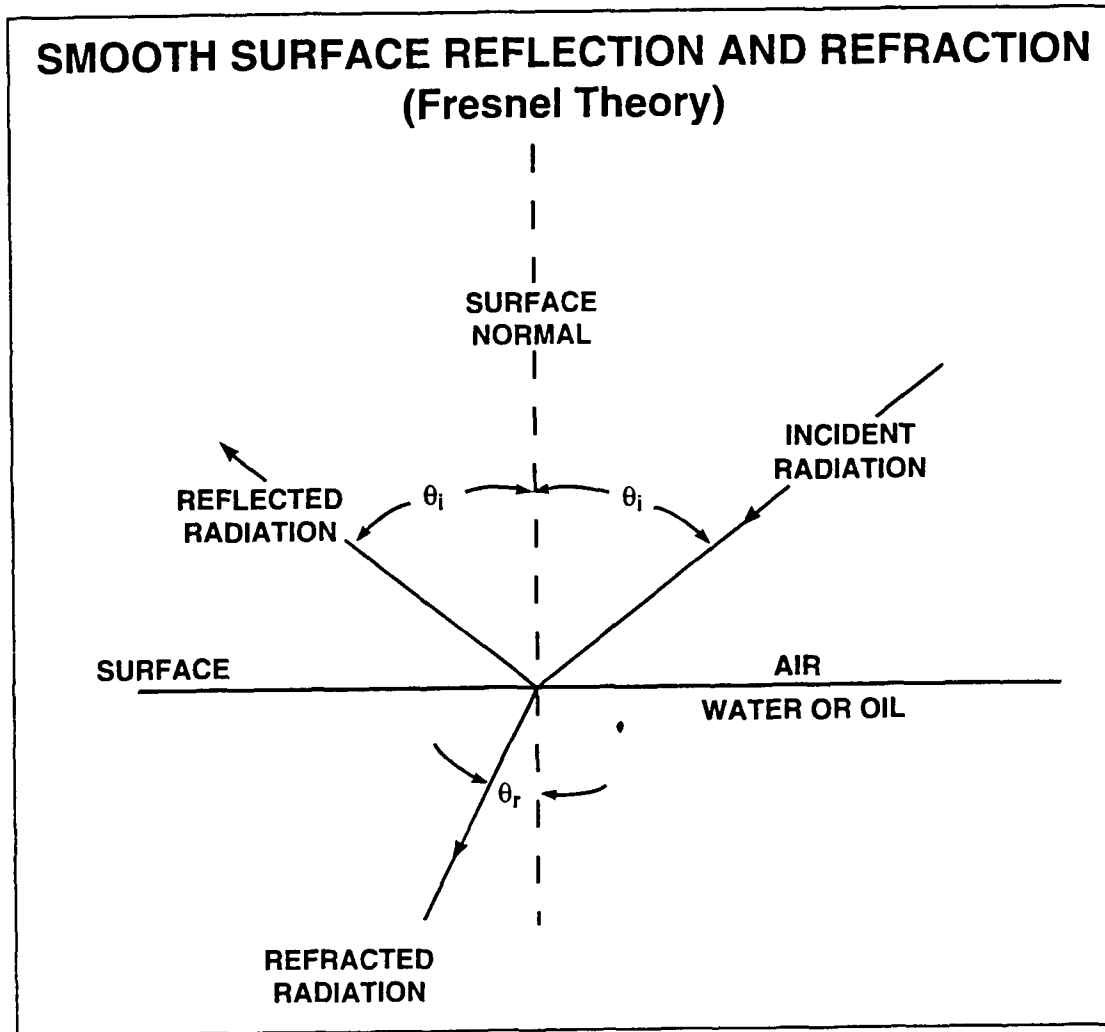


Figure 2-3. Smooth surface reflection and refraction (fresnel theory). The fraction of radiation reflected is determined by the bulk refractive index of the surface material,  $n$ , and the angle of incidence  $\theta_i$ . MWIR sensors will weigh 3.0-4.0 and 4.5-5.0 contributions dependent upon shape of detector material response curve.

are:

Normal Reflectance:

$$r_o(\Delta\lambda) = \left[ \frac{n(\Delta\lambda) - 1}{n(\Delta\lambda) + 1} \right]^2 \quad (2-5)$$

Refraction:

$$\sin \theta_r = \frac{\sin \theta_i}{n(\Delta\lambda)}, \text{ (Snell 's Law)} \quad (2-6)$$

Off-Normal Reflectance:

$$r(\Delta\lambda, \theta) = \frac{1}{2} \frac{\sin^2(\theta_i - \theta_r)}{\sin^2(\theta_i + \theta_r)} + \frac{1}{2} \frac{\tan^2(\theta_i - \theta_r)}{\tan^2(\theta_i + \theta_r)} \quad (2-7)$$

These equations are sufficient for the analysis.

The data base of  $n(\Delta\lambda)$  for various oils is rather limited. Table 2-1 gives normal emittances,  $\epsilon(\Delta\lambda)$ , for various oils and sea water in the infrared bands of concern here. Figure 2-4 is a sample calculation displaying the differences between oil and sea water emittance,  $\epsilon(\Delta\lambda, \theta)$  or reflectance as a function of angle for 44.7° API crude oil, the closest in refractive index to water and so the oil most difficult to detect of Table 2-1. The differences in the curves of Figure 2-4 are the primary factor determining the infrared observability of oil on water at night when oil and water will be very close in temperature. During the day oil will be differentially heated due to its strong absorption of sunlight. The analysis of this daytime situation is more complex, but such an analysis is not necessary for the purposes of this report. Simply stated, oil will appear much brighter (warmer) than water during the day, under solar illumination (see Section 2.6.)

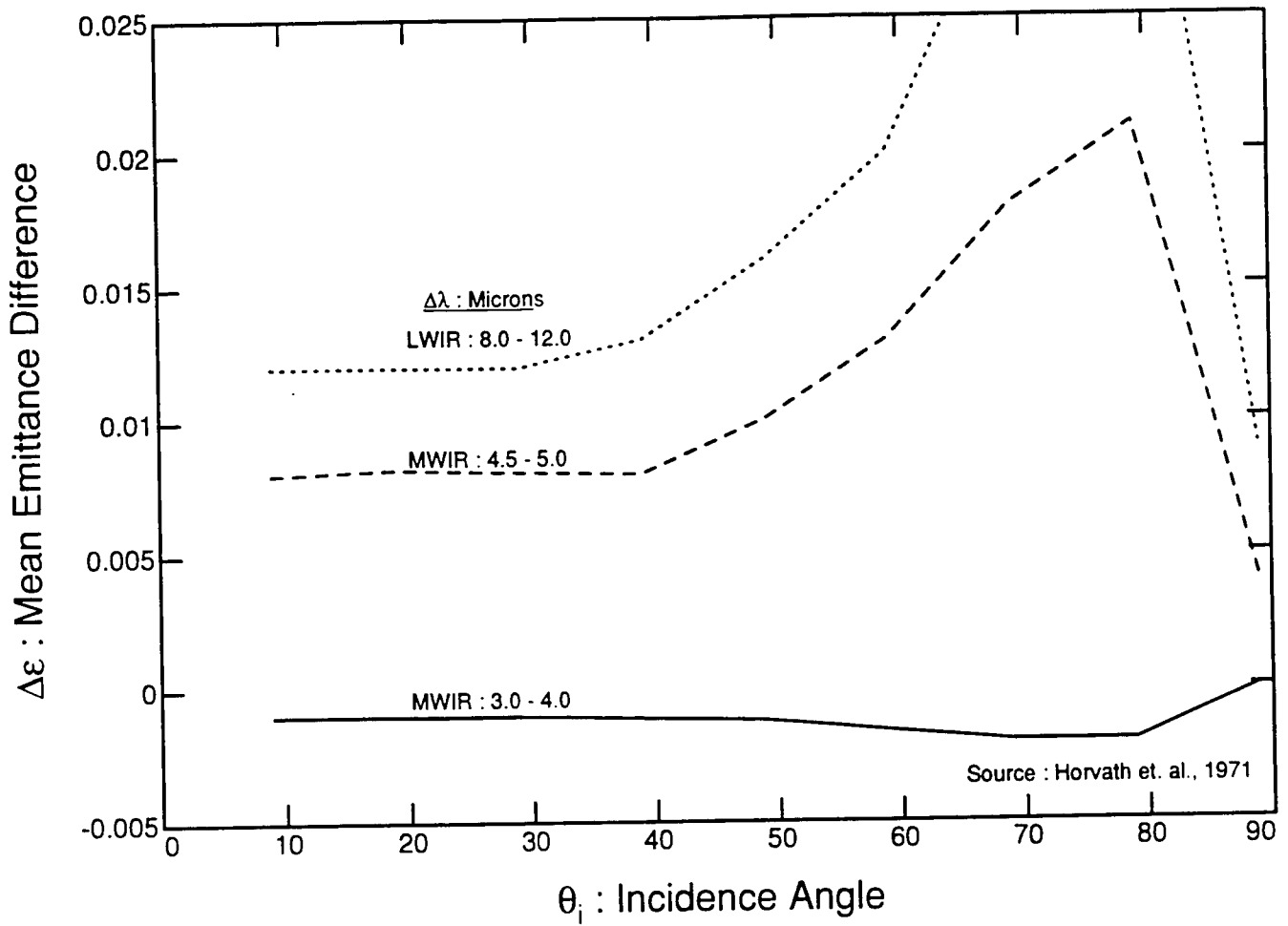


Figure 2-4. Emittance difference of oil and water vs angle of observation. This difference is the driver in determining the contrast radiance at night of an oil slick on water.

**TABLE 2-1**

**Normal Emittance of Oil and Water For Atmospheric Window Regions  
[reference 11]**

<u>Material</u>	<u>Wavelength Band (<math>\mu</math> m)</u>		
	<u>3-4</u>	<u>4.5-5.5</u>	<u>8-14</u>
100 - Octane Fuel	0.980	0.979	0.973
Kerosene	.968	.968	.968
Diesel	.968	.969	.972
SAE-30	.965	.965	.970
8.6° API Residual	.958	.958	.964
44.7° API Crude*	.973	.972	.973
31.3° API Crude	.969	.970	.967
19.5° API Crude	.969	.970	.972
Fish Oil	.969	.961	.959
Sea Water*	0.972	0.980	.985
*Used in analysis			

**2.3.2 Rough Surface and Volume Scattering**

The theory of Fresnel reflection just outlined is considered sufficient for the analysis effort needed for the assessment of oil spill detection at night with airborne FLIRs. Other mechanisms which may contribute marginally to IR thermal contrast signatures include: rough surface scattering, volume scattering and finite layer effects. Finite layer interference effects, briefly considered below in Section 2.3.3, are central to the FSR millimeter radiometry concept developed in a companion report [reference 2] but are not

relevant to FLIR use. Rough surface and volume scattering then are primarily of interest in the visible and near-infrared.

Figure 2-5 is a schematic indication of rough surface scatter; and Figure 2-6 is a similar schematic of volume scatter. Irregularities in the smooth surface of Figure 2-3 will introduce reflected wave distortions which will require a considerably more complex analysis than Fresnel Theory. In the limit of Lambertian (ideally rough) surfaces, the scatter will be uniform in all directions rather than specular. An example of rough (but not Lambertian) surface scatter of specific interest to imaging sensors which operate during the day at wavelengths from the ultraviolet to the near-infrared is Cox-Munk, or solar glitter, scatter, [reference 12]. This is light scattered from wind-driven capillary waves with characteristic sizes of a few centimeters. These phenomena can be analyzed in terms of specular scatter from a statistical distribution of Fresnel reflectors. Note, it is the absence of this nearly-omnipresent scatter from sea surfaces that allows the detection of oil slicks (which suppress these capillary waves) by back-scatter radars, [reference 3]. In the infrared the thermal emission from oil or water surfaces dominates these relatively small scatter effects. However, the effect in the infrared of this difference in rough surface scattering by oil and water should be small, at least in the absence of specular scattering of moonlight (which was not reported.) The oil-water contrast will be dominated by Fresnel emission and reflection.

Figure 2-6 schematically describes volume scatter. The observation of such scatter is an interplay of the density of suspended particulate matter which causes the scatter and the attenuation of scattered energy by the medium itself in the visible [reference 11]. Sea water has weak volume scatter per unit length in the visible, but also, low absorption of scattered radiation. Oils vary widely but strong volume scatter and strong absorption per unit length is expected from most (see Section 2.5). The contribution of volume scatter to oil-water contrast is then always a function of oil slick thickness and varies with the specific properties of oils and seas (e.g., microscopic organisms). Note that, in shallow

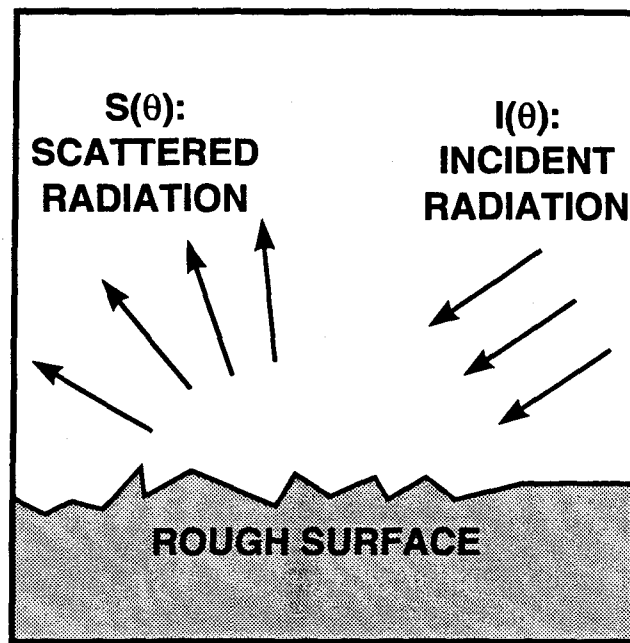


Figure 2-5: Rough surface scatter. In limit scattered radiation is "lambertian," that is scattered uniformly.

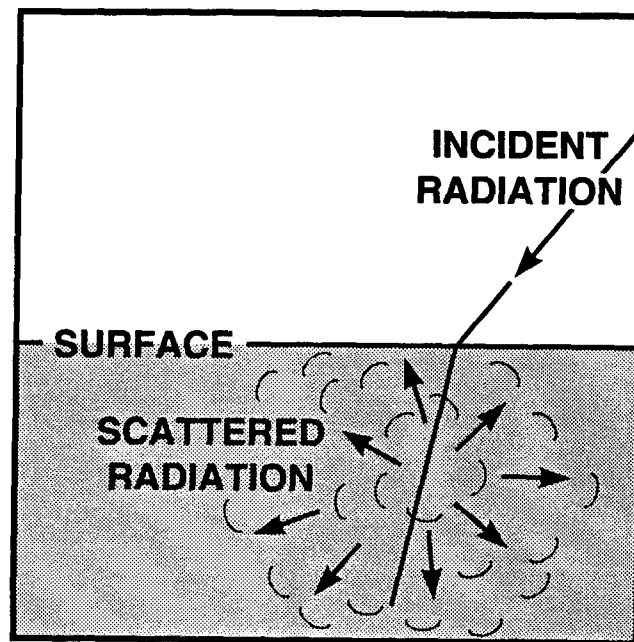


Figure 2-6: Volume scatter. The observability of volume scatter is an interplay of the material scattering coefficient per unit length and the material absorption coefficient per unit length.

water reflections from the sea bottom will be an additional complexity which may aid slick detection, since oil will absorb this reflected component quite strongly. Figure 2-7 is an example of volume backscatter in the visible at two ocean locations [reference 13]. Figure 2-8 is a sample of volume backscatter per unit length (i.e., per micron) for two oils [reference 11]. No simple generalization can be made from these curves on relative contributions of oil and water to volume backscatter in the visible. However, the sharp drop off with wavelength in both figures indicates the scattering particles are small and so volume scatter effects should be quite small at infrared wavelengths.

### **2.3.3 The Assumption of Optical Thickness**

It is important to state that the analysis of this report is done on the assumption that the oil layers or slicks of concern are "optically thick." The term "optically thick" means that the thickness of an oil layer is much greater than the absorption length of the layer (see Figure 2-11) in the sensor bandpass used. Specific measurements are not available to support this assumption. It is known that non-aromatic hydrocarbons (e.g., pentane, octane, etc.) have absorption features in the 3-4 and 8-12 micron spectral regions. Crude oils are a complex mixture of many non-aromatic hydrocarbons and so presumably absorb strongly (and so have small absorption lengths) in the MWIR (3-5 micron) and LWIR (8-12 micron) bands.

While specific supporting data are not available, it is the considered judgment of the authors of this report, supported by an analysis such as that of reference 2 and general background, that the assumption of optical thickness should be satisfactory for layers of thickness greater than about one-tenth of a millimeter. For thinner layers (down to several microns) reflections from the oil-water interface must be added to those of the air-oil interface (thick layer reflections) and interference effects should be considered. Oil-water contrast temperatures should fall between the thick layer calculations, Sections 3 and 5, and about one-half of those values. For very thin layers, of-the-order-of microns, a set of calculations should be made along the line of reference 2. The data analyzed



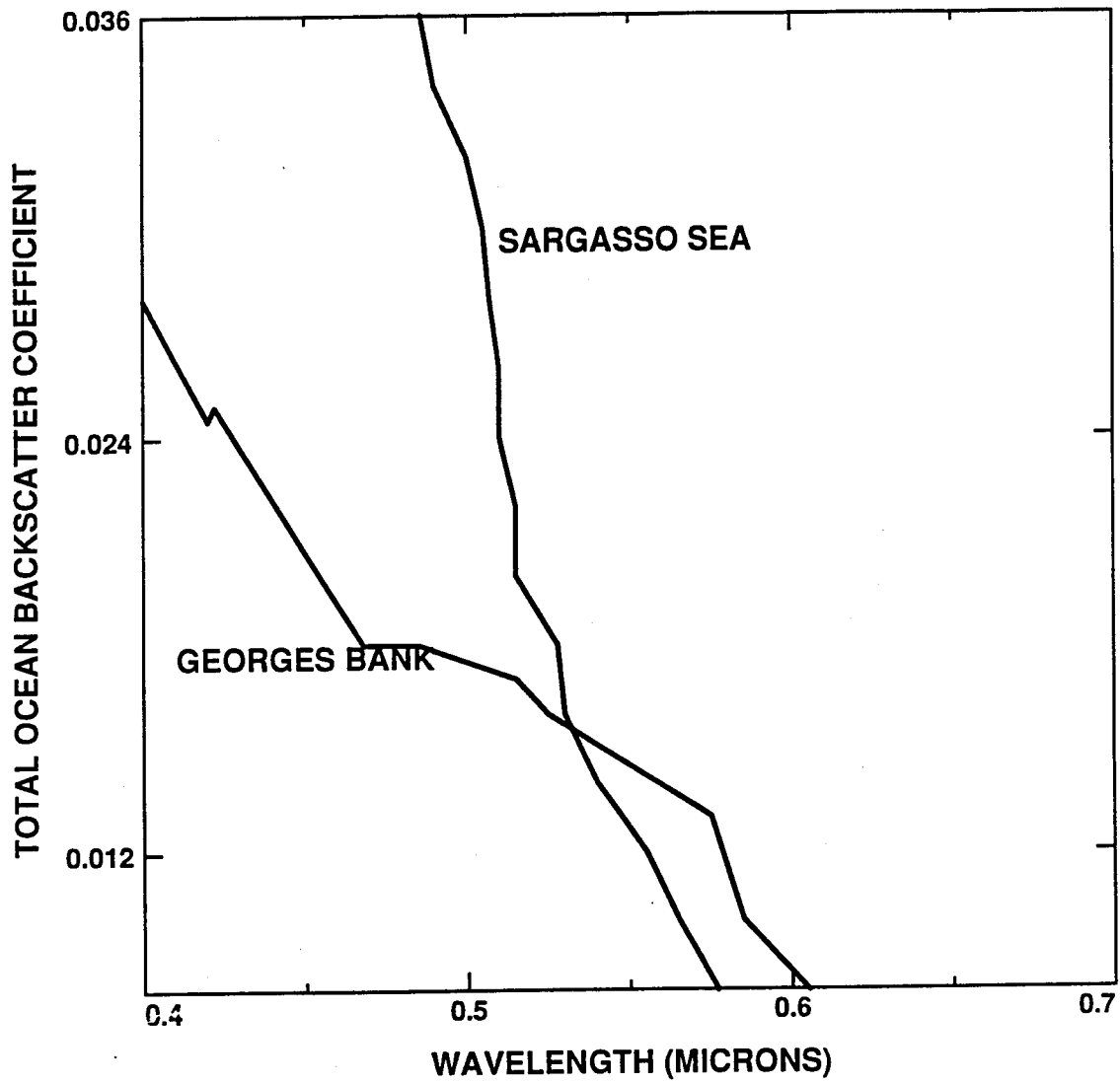


Figure 2-7: The spectra of back-scattered light from two ocean surfaces. Variability is caused by density of suspended bio-matter and other material.

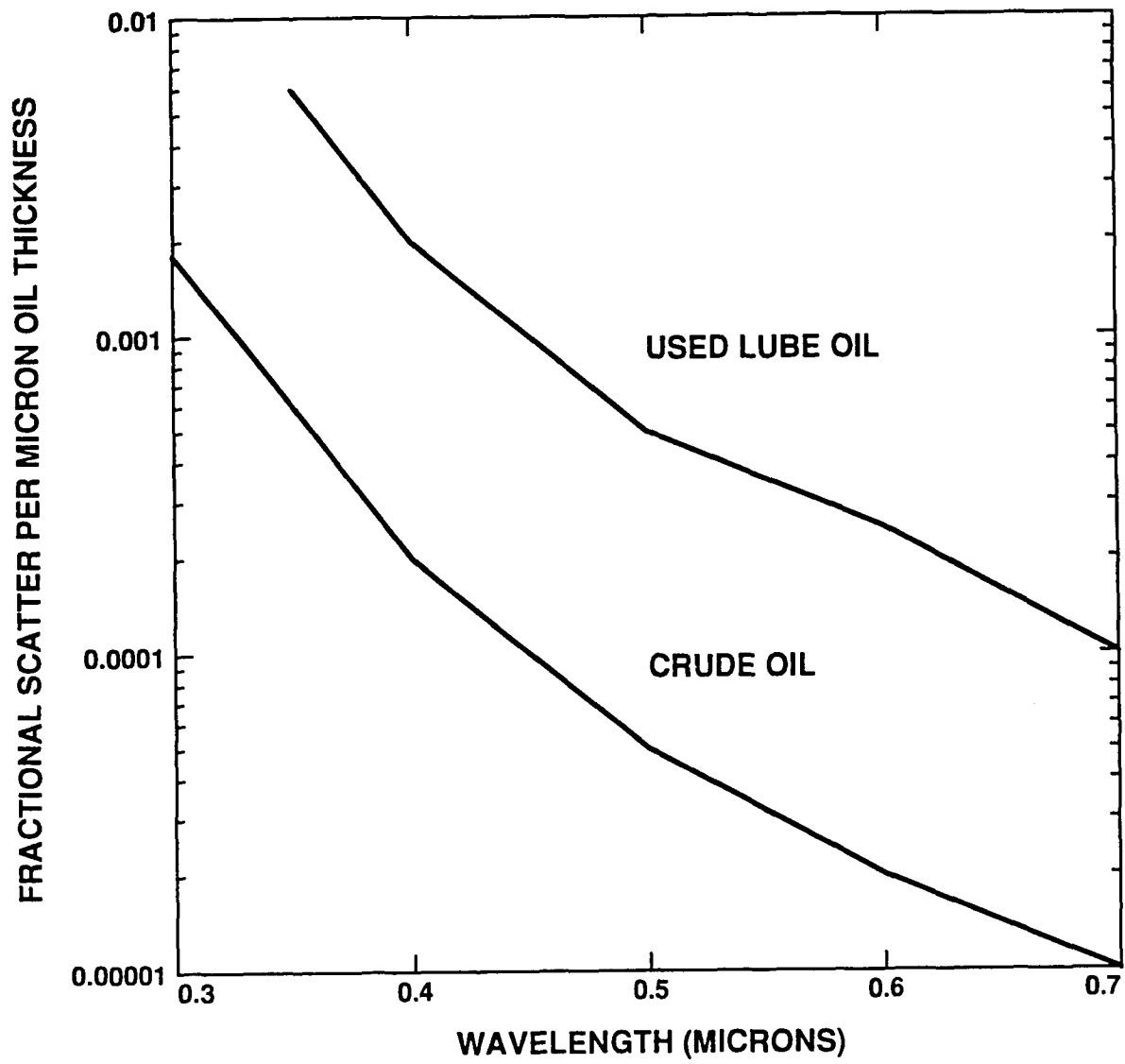


Figure 2-8: The spectra of the volume scattering coefficient of two oils involved.

here are from layers of several millimeters thickness as discussed in reference 1. Specific clean-up actions are usually only useful for layers greater than a few tenths of a millimeter. Thus the assumption of optical thickness and the contrast calculations of Sections 3 and 5 should be applicable to the test data of Section 5 and most oil slicks of operational (i.e., clean-up) interest. For thinner layers these calculations result in an overestimate of contrast by something less than a factor-of-two. However, since a particularly stressing set of oil parameters was made in the contrast calculations (see Section 3) the results should be applicable to a satisfactory approximation for the purposes of this report.

#### **2.3.4 Finite Layer Effects**

For completeness the phenomenology of finite layer effects must be considered here - but only in passing. By a finite layer is meant a layer whose physical thickness is comparable to or less than the characteristic absorption length of the medium, that is a layer that is not "optically thick." For a finite layer the possibility exists of reflection (or emission) being detected from the bottom surface interface (presumably of oil with water) as well as the top interface (of oil with air). The two finite layer phenomena of primary interest are interference and differential absorption. These effects may be exploited to estimate layer thickness and must be accounted for in interpreting all reflection data. To estimate layer thickness one requires that observations be made in a narrow spectral band, that is:  $\Delta\lambda \ll \bar{\lambda}$ , where  $\bar{\lambda}$  is the average wavelength in the band  $\Delta\lambda$ . Such a situation occurs in the application of FSR at millimeter wavelength (Section 1-5) where this layer interference phenomenon is exploited to estimate thickness [reference 2]. Finite layer effects are readily observable in the rainbow effect seen in reflected sunlight by oil films on pavements or water pools. Also it is, in principle, possible to estimate thickness from differential absorption effects. The reflection from a layer is the sum, (ignoring interference) of reflections from the top interface of the layer with air and the bottom interface with water. If the absorption per unit length of a layer varies strongly with  $\bar{\lambda}$  then the dependence of such reflection (or oil-water contrast) on  $\bar{\lambda}$  is an indicator of oil

thickness. Such a measurement might be made by a tunable laser as touched on in Section 6.2.

It will be found in Sections 3 and 5, that calculated oil-water nighttime contrast temperatures are appreciably greater in the LWIR than in the MWIR. Thus, LWIR imagers (given roughly the same sensitivity) are, in principle, preferred over MWIR sensors, given the assumption of oil layer optical thickness upon which the analysis of Sections 3 and 5 is based. This need not be true for these layers, particularly those layers that might be seen from natural oil seepage. For such layers it is the ratio of layer thickness to sensor mean-wavelength that measures the effect of layer thickness. This is, by definition, smaller for the LWIR ( $\lambda \sim 10$  microns.) Thus, oil-water contrast features, though reduced relative to thick layer calculations, might be more pronounced in the MWIR than in the LWIR, and MWIR sensors might be preferable for oil seepage detection, that is for layers a few microns thick and less. Such calculations are beyond the scope of this report and not further considered here.

## **2.4 THERMAL RADIATION: THE PLANCK FUNCTION**

The Planck function,  $P(\lambda, T)$ , gives the spectral radiance (watts/cm<sup>2</sup>-microns steradian) emitted by a "black-body," that is a perfect surface emitter, as a function of its sole determinants: wavelength,  $\lambda$ , and surface temperature  $T$  [reference 13]. Its derivation by Max Planck in 1900 was the first use of the photon hypothesis, the second being Einstein's photoelectric theory in 1905, and the third being Bohr's planetary atom in 1912. The integral of  $P(\lambda, T)$  over a sensor passband,  $\Delta\lambda$ , is the Planck integral of Equation (2-3). Together with Equations (2-4) to (2-6) and the physics and phenomenology of atmospheric radiation embodied in the LOWTRAN code (Section 2.5) it comprises the essential physics basic to this analysis.

The Planck function is given by reference 14 as

$$P(\lambda, T) = C_1 \lambda^{-5} / [\exp(C_2 / \lambda T) - 1] \quad (2-8)$$

where in  $C_1$  and  $C_2$  are scale constants dependent upon units used. Figure 2-9 is a plot of  $P(\lambda, T)$  versus  $\lambda$  for several values of  $T$ . These curves describe the thermal heat of radiation from ideal (black) or Planckian emitting surfaces. The radiation of Equation (2-8) is strongly dependent upon and, for a fixed wavelength, increases monotonically with temperature. The radiation from both the sun and the thermal radiation from the earth's surface (and oceans and oil slicks) can be approximated using Equation (2-8). The radiation from a given scene, observed in a wavelength band,  $\Delta\lambda$ , will be a sum of: reflected solar radiation, thermal self-emission, and reflected atmospheric radiation. Figure 2-10 is a comparison of the radiation from the sun at earth's surface with earth's thermal emission,  $P(\lambda, T)$  assuming a  $288^\circ \text{K}$  ( $15^\circ \text{C}$ ) average midlatitude temperature with unit emissivity, and with the thermal radiation incident on the earth's surface from the atmosphere  $I(\lambda, T)$ .

The solar component, when solar zenith angle and typical surface reflectances are taken into account, will be reduced by (very roughly) a factor-of-ten for an observer viewing a scene. The thermal radiation will be reduced by typical surface emissivities to 80-90% of the  $P(\lambda, T)$  values of Figure 2-10. It can be seen then that the overlapping region between solar emission (day) and thermal surface emission is small (the 3-4 micron region). Sensor systems then tend to divide (to oversimplify) between those dependent upon reflected sunlight (or moonlight) which operate at wavelengths below about 2 microns and those relying on thermal emissions which operate above 3 microns. The atmospheric radiation curve of Figure 2-10 was calculated with LOWTRAN-7 (Section 2.5). The integrals of this curve over the appropriate wavelength limits ( $\Delta\lambda$  sensor bandpass) are the incident radiation terms,  $I(\Delta\lambda, \theta)$ , of Equation (2-3) and Figure 2-3. The integral of the black-body curve corresponds to the  $P(\Delta\lambda, T_s)$ , thermal emission terms of Equation (2-3). The determination of  $\tau(\Delta\lambda)$  and  $\epsilon(\Delta\lambda)$  have been discussed in Section 2.3.1.

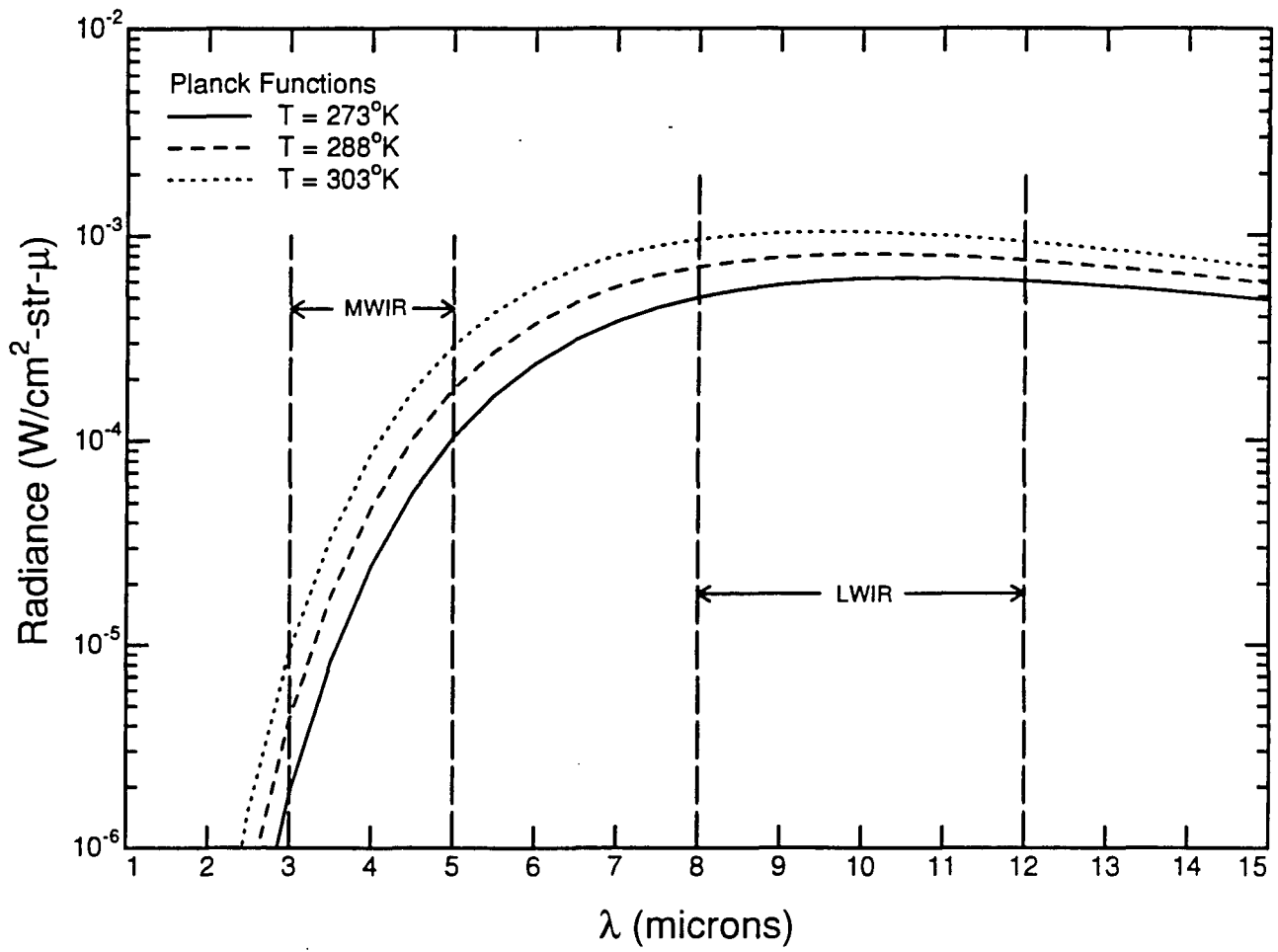


Figure 2-9. Planck radiation curves for temperatures typical of standard environments.

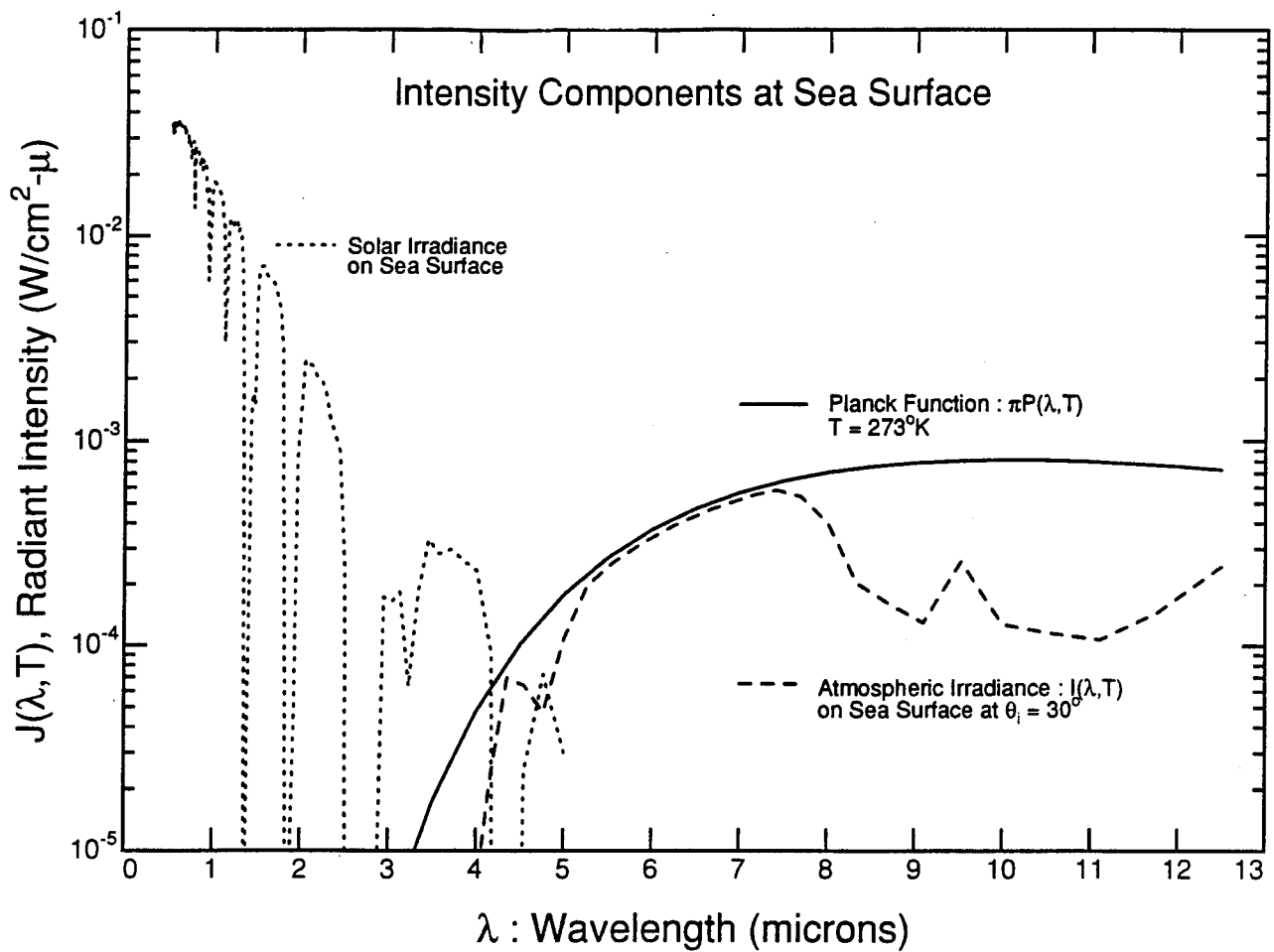


Figure 2-10. Comparison of the intensity components incident on and emitted by sea surface at standard conditions. Note, for proper comparison of components the planck spectral radiance has been multiplied by  $\pi$ .

## **2.5 THE LOWTRAN CODE**

A quite general computer code supporting infrared radiometric measurements in the atmosphere has been developed by the Air Force Geophysical Laboratory (Phillips Laboratory) at Hanscom Field, Bedford, MA. [reference 15]. For nearly arbitrary atmospheric conditions (e.g., altitude profiles of humidity, temperature, precipitation, clouds, etc.) the code, which is called LOWTRAN, can be used to predict the absorption of any atmospheric path, and the radiation from the atmosphere, earth, sea, sun or moon seen at any observing geometry. Development of the code has stretched over several evolutionary steps spanning twenty-five years. The latest (and probably final) version is call LOWTRAN-7. The code can be taken as a standard for a wide range of civilian and military uses. Its accuracy, at least in the lower atmosphere, has been adequately demonstrated for most systems applications.

## **2.6 OIL AND WATER SURFACE TEMPERATURES**

The surface temperature,  $T_s$ , of the ocean needed for Planck radiation calculations, varies from its freezing point,  $\sim 0^\circ \text{C}$ , in Arctic regions to about  $30^\circ \text{C}$  at the equator. This temperature is controlled primarily by the temperature of underlying waters and to a lesser extent by solar irradiation and convective and evaporative cooling which are dependent upon winds. The temperature of a shallow pond (the situation of the data base discussed in Chapter 4) will be considerably more dependent upon the sun and winds. The temperature of an oil slick on water at night will be essentially the same as the surrounding water with, perhaps, slight differences dependent upon details of evaporative cooling, [reference 16.] In the day, oil temperature can be several degrees higher than water because of the much stronger sunlight absorption coefficient of oil. Figure 2-11 compares the spectral absorption length of water an oil in the visible and near-infrared, [references 11 and 17]. This tells us that a relatively thin layer of oil will absorb a much larger proportion of available solar energy than the upper layer of the surrounding ocean. The effect of this will be a pronounced differential heating and temperature increase of



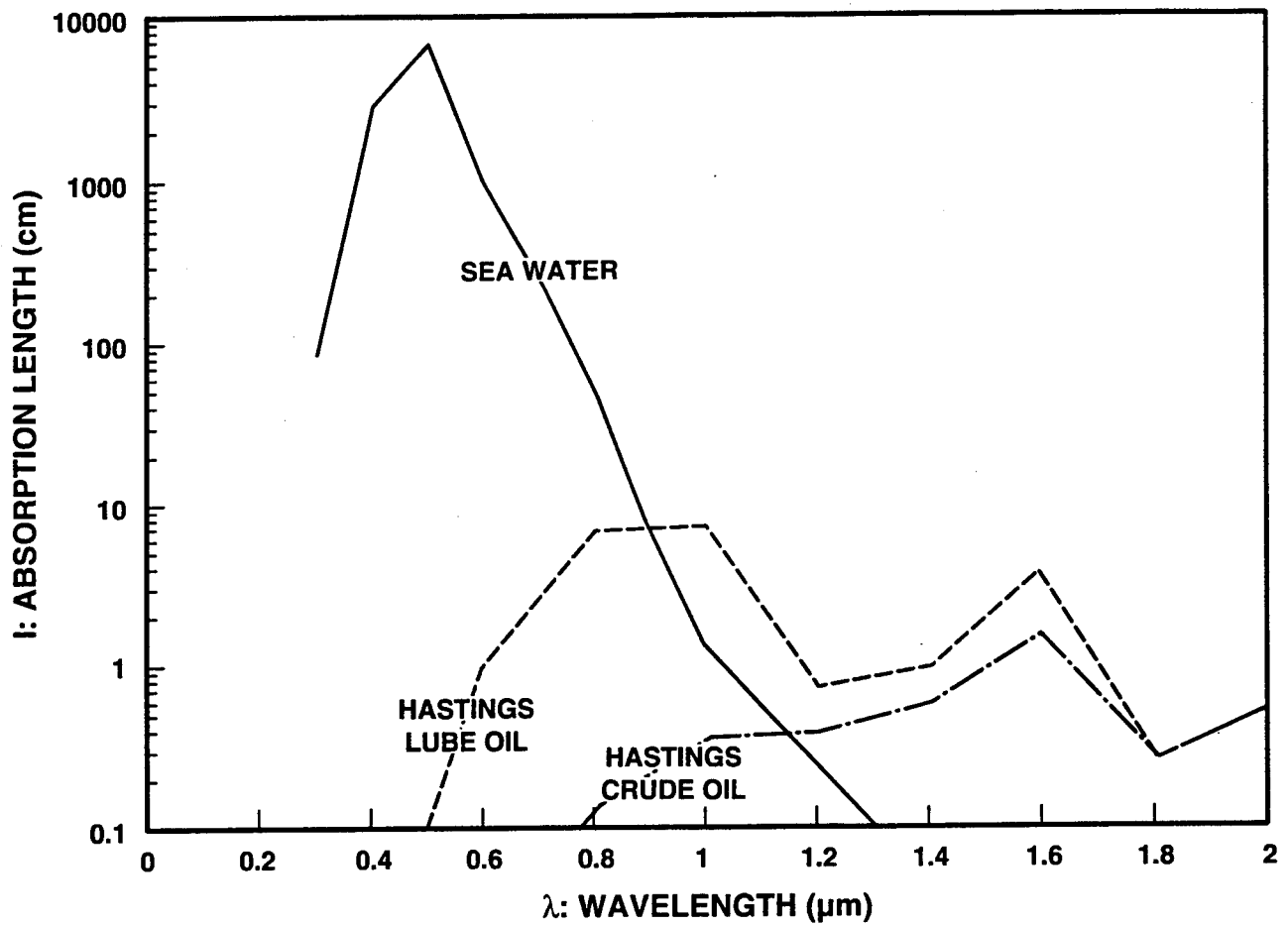


Figure 2-11. Characteristic absorption lengths of sea water and two oils. Oils will strongly absorb visible light and so be differentially heated relative to water during the day.

oil. The consequent differential temperature was seen in the infrared imaging data taken during daytime overflights of test slicks discussed in Section 5.3.

The theory of oil slick temperatures is discussed by Horvath [reference 11], and that of water temperature by Eagleson, [reference 18]. For the purposes of this report we take the oil and water temperatures as being equal at night, and the oil temperature as being a few degrees (see Section 5.4) higher than water during the day.

## CHAPTER 3

### INFRARED CONTRAST TEMPERATURE CALCULATIONS

#### 3.1 PROCEDURE

The term "radiometric temperature" of a feature means that black-body temperature,  $T$ , in the Planck function of Equation (2-8) which would give the same intensity integrated over a band  $\Delta\lambda$ , as actually measured by a sensor with a bandpass,  $\Delta\lambda$  observing that feature. This measured intensity, as in Equation (2-3), need not be purely thermal (that is Planckian) radiation. The ("measured") contrast temperature is then the difference between the radiometric temperatures of oil and water. This contrast temperature can be calculated from the theory outlined in Section 2, given the various input parameters and environmental conditions. These parameters are:

- $n$  (oil),  $n$  (water) - the refractive indices of oil and water,
- $h, \theta$  - the sensor aircraft height and incident viewing angle (see Figure 2-1) and
- $T_s$  - the surface temperature of water and oil, assumed to be the same at night.

The environmental conditions (season, latitude, weather) are themselves inputs to LOWTRAN-7 calculations from which are obtained values of: transmission,  $\tau(\Delta\lambda, h, \theta_i)$ , and atmospheric radiance,  $I(\Delta\lambda, \theta_i)$ , used in Equation (2-3). This theoretical modeling procedure is schematically represented in Figure 3-1.

The results of such calculations can be presented in different ways. It seems most useful here to calculate plots of oil-water contrast temperature as a function of viewing angle,  $\theta_i$ , for the MWIR and LWIR sensor bands. A distinction is made in the MWIR between sensors with PtSi (Platinum Silicide) detector arrays and sensors with InSb (Indium

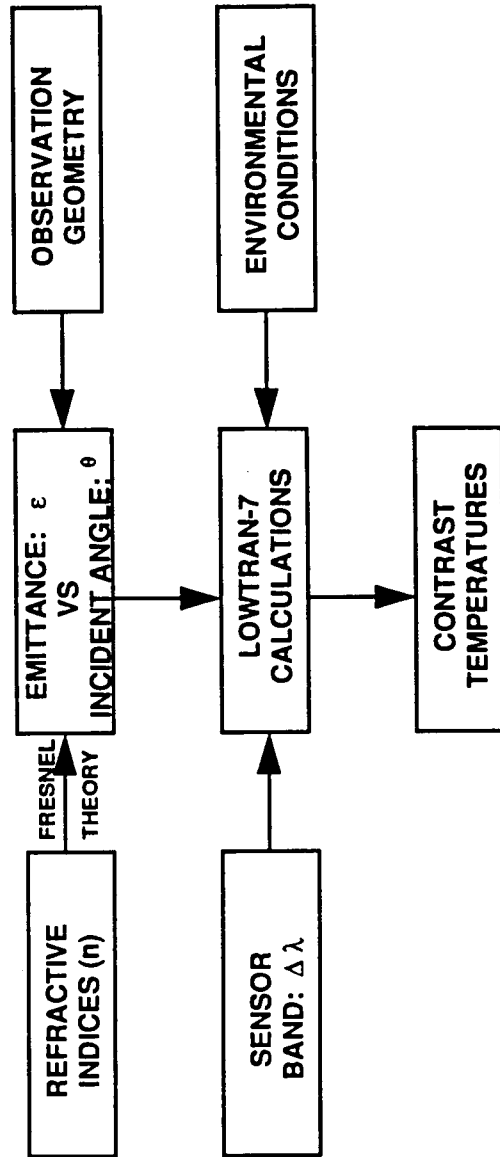


Figure 3-1. A block diagram of contrast temperature calculation procedures.

Antimonide) or PbSe (Lead Selenide) detector arrays. This distinction is based upon differences between the wavelength dependence of their sensitivity over the 3-5 micron band. This distinction is fairly minor and is included in the calculations but not discussed here. Specifications for the particular sensors tested by the Coast Guard will be presented in Section 4.3.

### **3.2 CONTRAST AS FUNCTION OF SEASON AND LATITUDE**

In the calculations below, transmission,  $\tau$ , integrated thermal radiation,  $P(\Delta\lambda, T)$ , and atmospheric radiance  $I(\Delta\lambda, \theta)$  all vary strongly with season and latitude for the same observing geometry. Contrast intensity is, however, fairly insensitive to season and latitude because the variations tend to cancel as can be seen from Equations (2-2) and (2-3) and the following. Increases in surface temperature,  $T_s$ , and so thermal radiation,  $P(\Delta\lambda, T_s)$ , directly correlate with increases in atmospheric temperature and so,  $I(\Delta\lambda, \theta)$ . Further atmospheric radiation increases in both these quantities correlate with higher atmospheric absorption due to higher atmospheric humidity, and so decreases in  $\tau(\Delta\lambda, \theta)$ . The effect of these correlated variation results, as seen below, in nighttime water-oil contrast temperatures that vary by no more than a factor of two over a wide range of conditions.

Plots of contrast temperature vs incidence angle,  $\theta_i$  as seen by a sensor on an aircraft at constant height,  $h$ , above ground level (AGL) are taken as the mode for presentation of these calculations. A nominal height of 500 ft AGL was chosen for the calculations presented here. The results presented graphically in this subsection are for the five standard atmospheres which are incorporated in the LOWTRAN-7 program for calculating atmospheric radiance,  $I(\Delta\lambda, \theta_i)$ , and atmospheric path transmission,  $\tau(\Delta\lambda, \theta_i, h)$ . The atmospheres are: tropical, midlatitude summer, midlatitude winter, arctic winter, and 1976 standard (a midlatitude annual average for U.S.). The pertinent surface meteorological

properties of these atmospheres are given in Table 3-1. In the next subsection the effect of fog and rain will be treated. Figure 3-2 and Figure 3-3 give the results of these seasonal calculations for: the LWIR, 8-12 micron bandpass, and the MWIR, 3-5 micron bandpass. There are two curves for the latter bandpass because, as stated, the sensors of concern included devices using detectors (PtSi, InSb, and PbSe) with different wavelength dependent characteristics. It can be seen that there are only modest seasonal or latitudinal variations in predicted oil-water contrast temperatures because of the compensating variations of the individual terms in Equation (2-3) discussed above. Seasonal/latitudinal effects are more pronounced in the MWIR, but when one includes the dependence of MWIR sensor sensitivity on scene temperature to be discussed in (Section 4.2) this variability is also suppressed.

**TABLE 3-1**  
**METEOROLOGICAL PARAMETERS OF LOWTRAN**  
**STANDARD ATMOSPHERES [ref 15]**

<u>ATMOSPHERE</u>	<u>SURFACE TEMPERATURE °C</u>	<u>RELATIVE HUMIDITY (%)</u>
Tropical	26	76
Mid-Latitude Summer	21	76
Mid-Latitude Winter	0	77
Sub-Arctic Winter	-16	75
U.S. Standard	15	46

The contrast temperature curves are all fairly flat out to about 50° of incidence, then increase up to about 80° of incidence because of the increase in oil-water emissivity difference Figure 2-4 and the increase in atmospheric radiation (Figure 2-3) with increasing  $\theta_i$ . The curves then decrease sharply because of the drop in atmospheric transmission,  $\lambda$ , with rapidly increasing range at 80°-90° of incidence (see Figure 3-5 below.) The LWIR contrast levels are of the order of 1°K, while the MWIR contrasts are much lower, of the order of 0.1°K. These calculations were made for a stressing

(minimum difference in emittance) selection of oil refractive index, specifically the 44.7° API crude oil of Table 2-1. Thus, these contrast temperature calculations should be conservative - that is, low relative to most oils. If other crude oils were chosen from Table 2-1 one might have contrast temperatures up to about 50% higher than Figures 3-2 and 3-3.

### 3.3 THE EFFECT OF RAIN AND FOG

Fog and rain will suppress oil-water contrast temperatures for two reasons: the decrease in atmospheric transmission,  $\tau$ , of the observing path, and the reduction of the clear atmosphere contrasts of Equation (2-3) due to increases in the atmospheric radiation,  $I(\Delta\lambda_1\theta_i)$ . Using LOWTRAN modeling the effects are displayed in Figure 3-4 for the LWIR; the situation for the MWIR is similar. A standard atmosphere has been assumed; and the contrast temperatures are calculated for light rain, heavy fog (approximated as a standard advective fog) and light fog (approximated as a standard radiative fog.) The clear atmosphere calculations of Figures 3-2 and 3-3 are included as reference conditions. Rain is seen to reduce calculated contrast temperatures by two orders-of-magnitude and fog to reduce contrast by an order-of-magnitude. The effects of rain and fog on LWIR path transmission are displayed in Figure 3-5. The suppression of contrast temperatures by rain and fog as displayed in Figures 3-4 and 3-5 results in temperature contrasts in the LWIR (and MWIR) which are well-below sensitivity thresholds of available sensors.

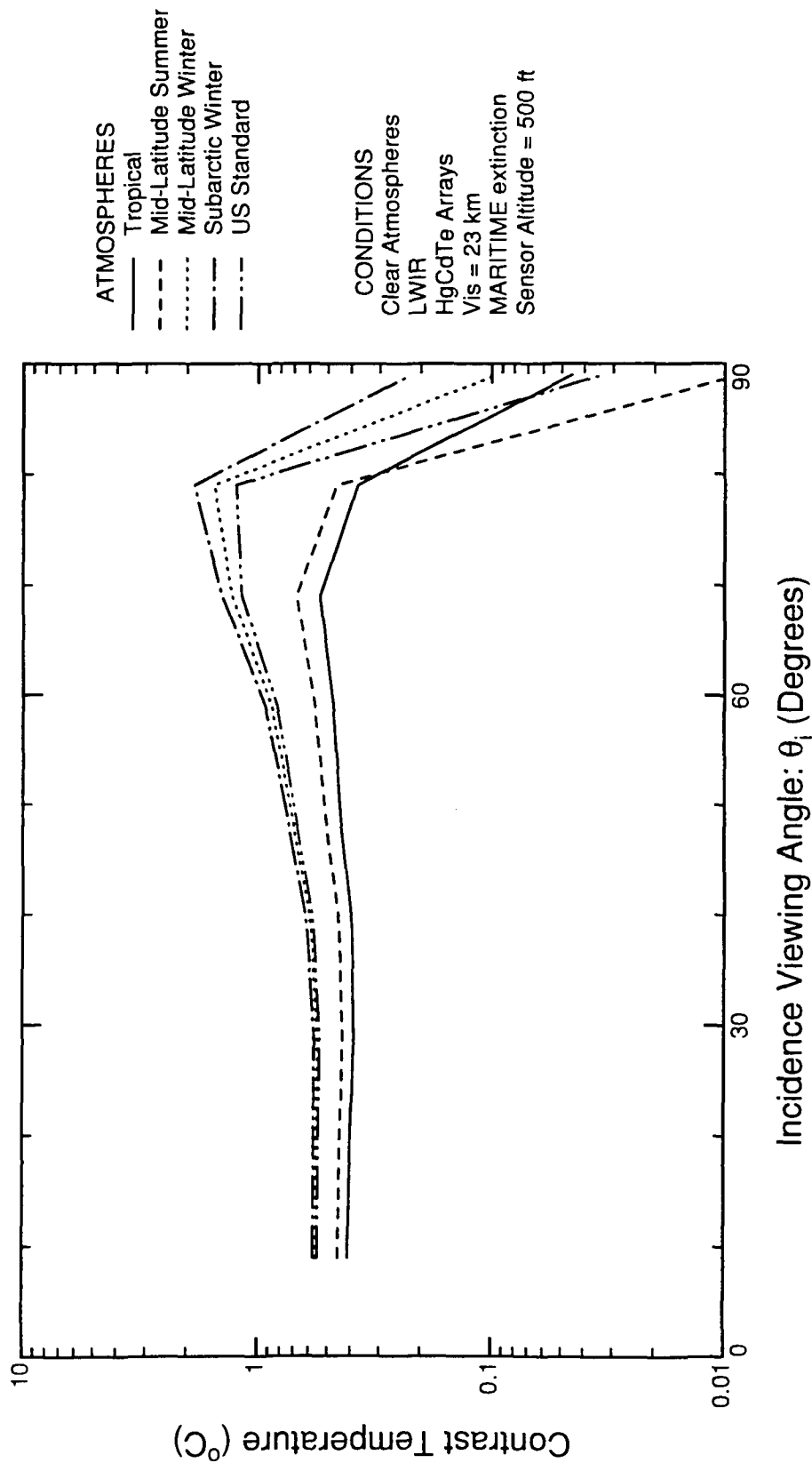


Figure 3-2. Predicted LWIR nighttime water-oil contrast temperatures. Calculations are made for a set of standard atmospheric environments.



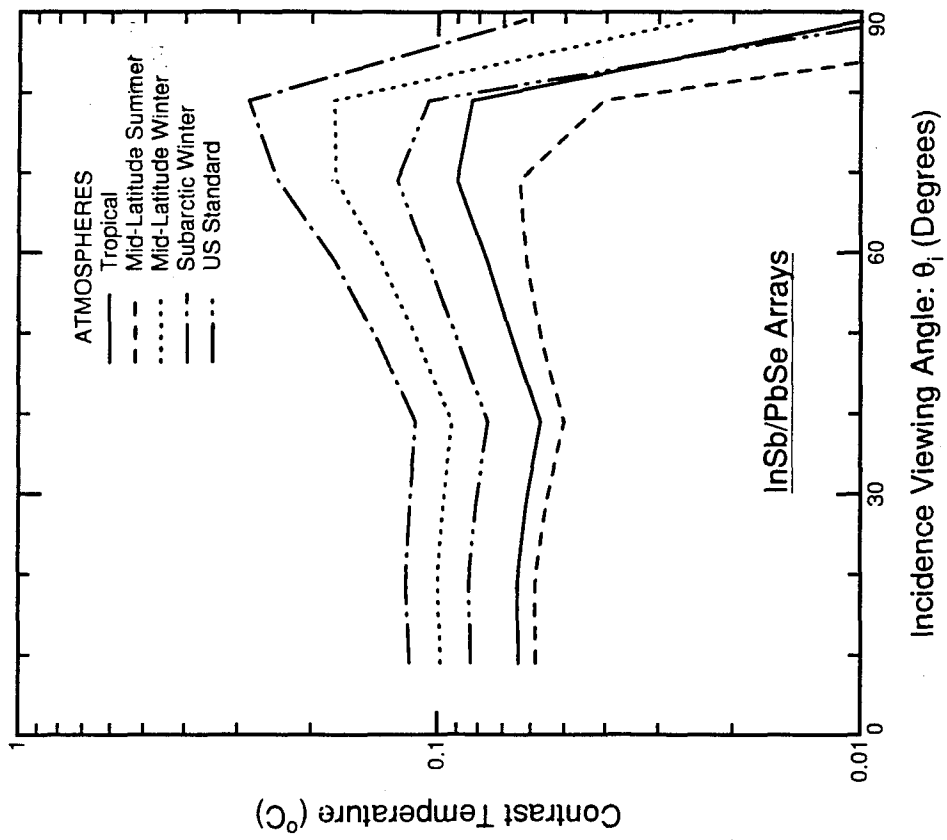
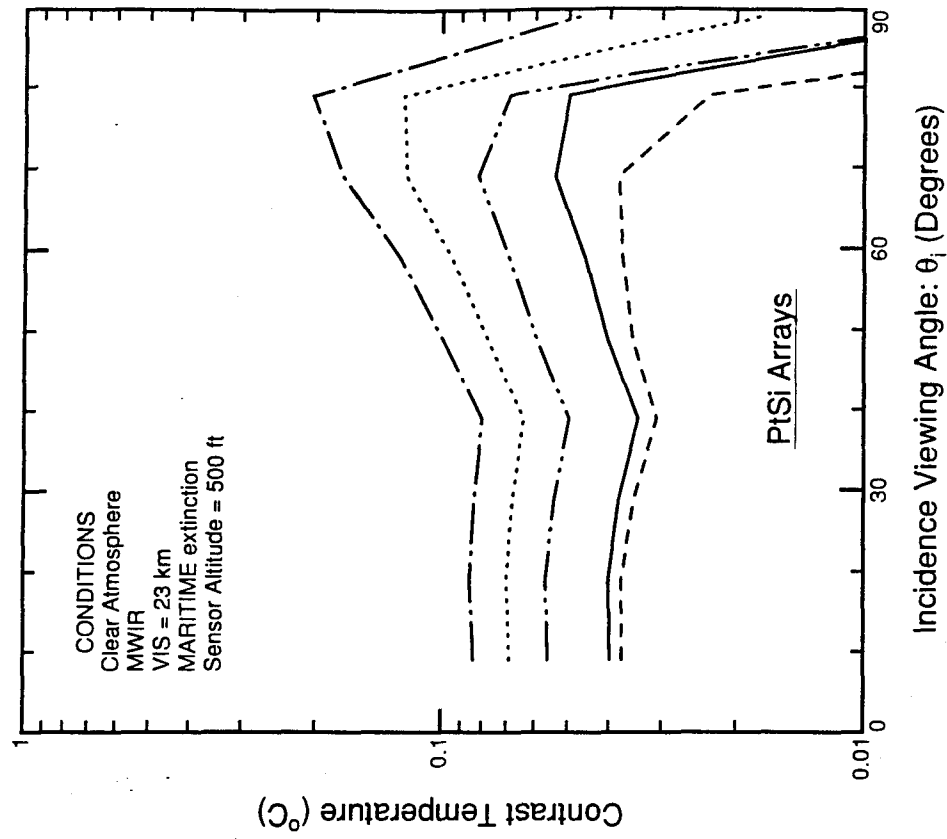


Figure 3-3. Predicted MWIR nighttime water-oil contrast temperatures. Calculations are made for a set of standard atmospheric environments and two MWIR detector material types.

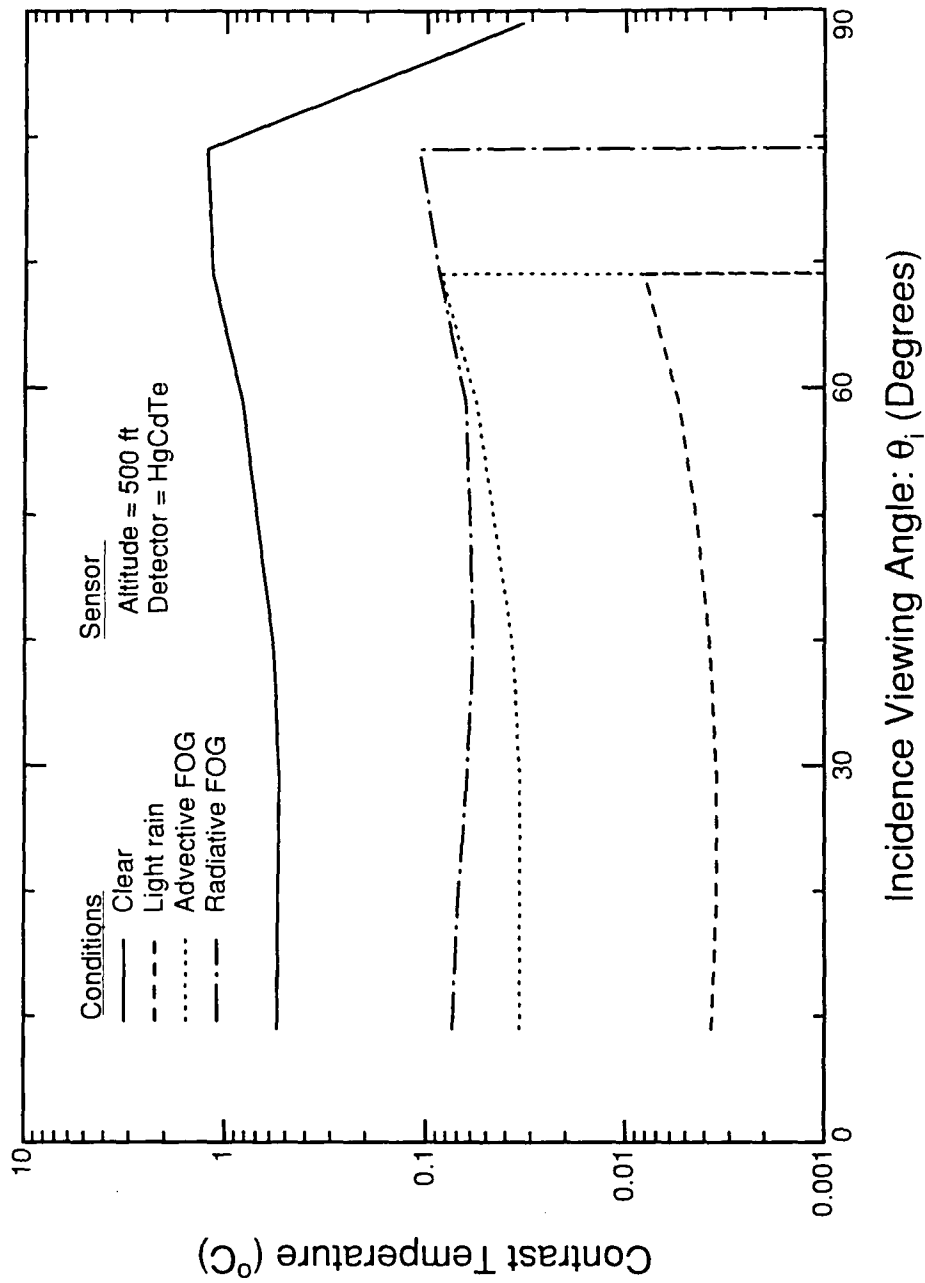


Figure 3-4: The effects of fog and rain on predicted LWIR water-oil contrast temperatures.

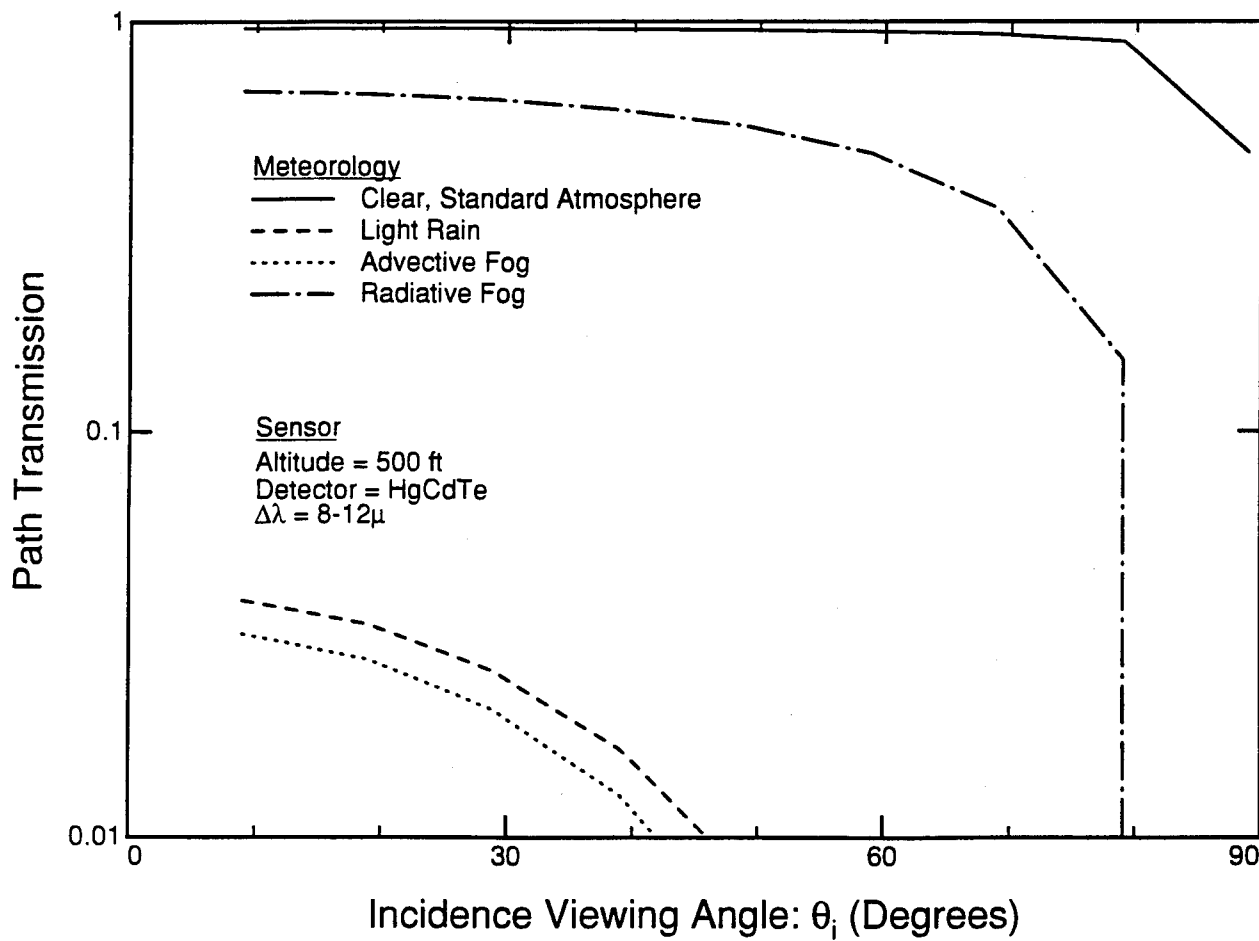


Figure 3-5: The effects of fog and rain on LWIR atmospheric path transmission.

## **CHAPTER 4**

### **DATA**

#### **4.1 USCG TEST PROGRAM**

During May 1993 the U.S. Coast Guard (USCG) participated in a field exercise conducted at the Canadian Forces Base, Petawawa, Canada. The Emergencies Science Division of Environment Canada (EC) planned the test to evaluate the ability of prototype, airborne, laser-acoustic and laser fluorosensor devices to detect, identify and quantify oil slicks. The USCG, R&D Center was invited to use the test site to evaluate other oil spill sensors of interest. The test program and the data base obtained by the USCG is described in detail in a companion report, [reference 1] and briefly summarized here.

Imaging data from the sensors described Section 4.2 were taken during the day on May 4, 5 and 6, and nighttime data were taken on May 4 and 5. This latter data set is of concern to this analysis. This data base was acquired with two gimbal-mounted LWIR sensors (8-12 microns) and three hand-held MWIR sensors (3-5 microns). These sensors were not calibrated. Images were recorded on a pool complex 480 feet long and 100 feet wide. The complex consisted of twelve pools, all of which contained water to a depth of about six inches; three were left as controls while the other nine contained several types of oil slicks with various thicknesses and times of aging. These slicks partially covered the water pools and moved with the prevailing winds. The details of these distributions are not germane to the work of this report. The pertinent optical properties, specifically the refractive indices in the infrared, were not known and so the oils are treated generically here. Refractive index is assumed for a representative, but stressing, oil using Table 2-1 and Equation (2-5).

A great deal of ground-truth data on oil slick thickness, water temperature, air temperature, relative humidity, and wind speed and direction were also collected. The temperature and humidity data are used for the contrast calculations of Section 5.2.

Details of this data base are given in [reference 1]. Table 4-1 summarizes the nighttime imagery data base pertinent to this analysis. The comments column refers to an assessment of the sensor data quality for the needs of this analysis.

**TABLE 4-1**  
**Nighttime Contrast Imagery Data Base**

Date	Sensor (See Table 4-2)	Comments on Contrast Imagery
May 4	FLIR 2000 (LWIR) WF-360TL (LWIR) IRC-160ST (MWIR) Agema 210 (MWIR) FSI Prism (MWIR) Night Vision Camera (Visible)	Fair-to-Good Fair-to-Good Poor Poor at Best Poor at Best Deceptive
May 5	FLIR 2000 WF-360TL IRC-160ST Night Vision Camera	Fair Good Fair Deceptive

#### **4.2 IMAGING SENSORS AND CONTRAST TEMPERATURE**

The goal of this analysis is to assess the relative utility of various imaging sensors for the detection of oil spills at night. The spectral region of particular interest then is the thermal infrared, specifically the atmospheric windows from 3 - 5 microns (with an atmospheric absorption notch from 4.1-4.5 microns) and from 8 - 12 microns. The development of sensor systems in these bands has been driven by military and remote sensing needs. A wide array of system options is thus available to potential users.

The sensor systems of concern here are not automated in the sense that many military and environmental remote systems are. The oil spill detection sensors of concern here are "imaging" sensors with human operators. The systems are designed at the input for maximum contrast sensitivity given other system constraints, and at the output present an image compatible with the contrast sensitivity and response time of human vision. The systems are essentially airborne TVs which image a scene in the infrared and convert that image into the visible as seen on a TV screen by an operator. This approach uses the very extensive image processing capabilities of the human eye, but does introduce practical problems in maintaining contrast levels on the screen. On the one hand, one must avoid saturation at parts of the scene with high contrast, and on the other, one must maintain sufficient system contrast sensitivity for such low-contrast features as oil spills to be seen.

The heart of the modern IR imaging sensor is an array of "detectors," each of which is rectangular with linear dimensions in the 10-100 micron size range. The advance of this technology is marked by the production of larger and more "uniform" arrays. By uniform, it is meant, the detectors of an array have responsivities to incident radiation which vary little from each other.

The sensitivity of an IR imaging sensor is usually expressed in terms of the radiometric temperature difference (e.g., apparent black-body temperature difference) which can be detected by a human viewing the output screen of the sensor systems. For example, if the radiometric temperature of an element of water in a scene is  $288.4^{\circ}\text{K}$  ( $15.24^{\circ}\text{C}$ ), and the radiometric temperature of an adjacent oil patch is  $288.1^{\circ}\text{K}$  ( $14.94^{\circ}\text{C}$ ), then the contrast temperature is  $0.3^{\circ}\text{K}$  ( $0.3^{\circ}\text{C}$ ). For a human to see this difference on the sensor screen, the sensor system must have a sensitivity which is less than (that is better than)  $0.3^{\circ}\text{K}$ . This difference in radiometric temperature may be (and at night probably is) entirely due to the emissivity difference between water and oil, rather than an actual temperature difference.

IR sensor systems have contrast temperature sensitivities that are expressed in a minimum detectable radiometric temperature change:  $\Delta T$  ( $^{\circ}\text{K}$  or  $^{\circ}\text{C}$ ). What the systems actually measure, and are sensitive to, is a minimum detectable radiance change,  $\Delta J$ , (watts/cm<sup>2</sup> -ster). The relation between  $\Delta T$  and  $\Delta J$  depends upon, through the Planck function, an average radiometric temperature:  $T$ , and finally to a mean temperature of the scene (oil and water) being viewed. This dependence is displayed for the MWIR in Figure 4-1. Figure 4-1 demonstrates that, at lower scene temperature, greater radiometric temperature contrast is required to generate the sensor's minimum detectable radiance contrast than would be required at higher scene temperature. A similar plot for the LWIR would be much closer to a straight line and so contrast temperature sensitivity would be less sensitive to changes in scene temperature.

Equation (2-8) has been used to plot  $\Delta T$  vs background temperature in Figure 4-2, for a fixed sensor sensitivity,  $\Delta J$ , in the three IR bands of interest: 3.0-4.1, 4.5-5.0, and 8.0-12.0 microns. Note that  $\Delta T$  is fairly insensitive to the expected temperature variation of 273-303° K (0 - 30°C) in the LWIR, but moderately sensitive in the MWIR. Thus, in effect, MWIR sensors "lose" sensitivity (as expressed in terms of a contrast temperature sensitivity) as the physical temperature of the scene being viewed decreases.

### **4.3 INFRARED IMAGING SENSORS TESTED BY THE USCG**

Table 4-2 lists the FLIRS used in the Coast Guard field experiment together with their bandpasses and sensitivities, the parameters of specific concern to this study. This information was obtained from vendor literature. The two LWIR sensors are gimbal-mounted instruments flown on Coast Guard aircraft. The three MWIR sensors were used by the Coast Guard to assess the utility of various hand-held infrared images. For the most part the sensitivities of 0.1-0.2° C are those that have been available for some time in a variety of instruments. The IRC-160ST MWIR sensor represents an advanced state-of-the-art instrument. Its excellent sensitivity (0.04°C) is the result of the large focal plane

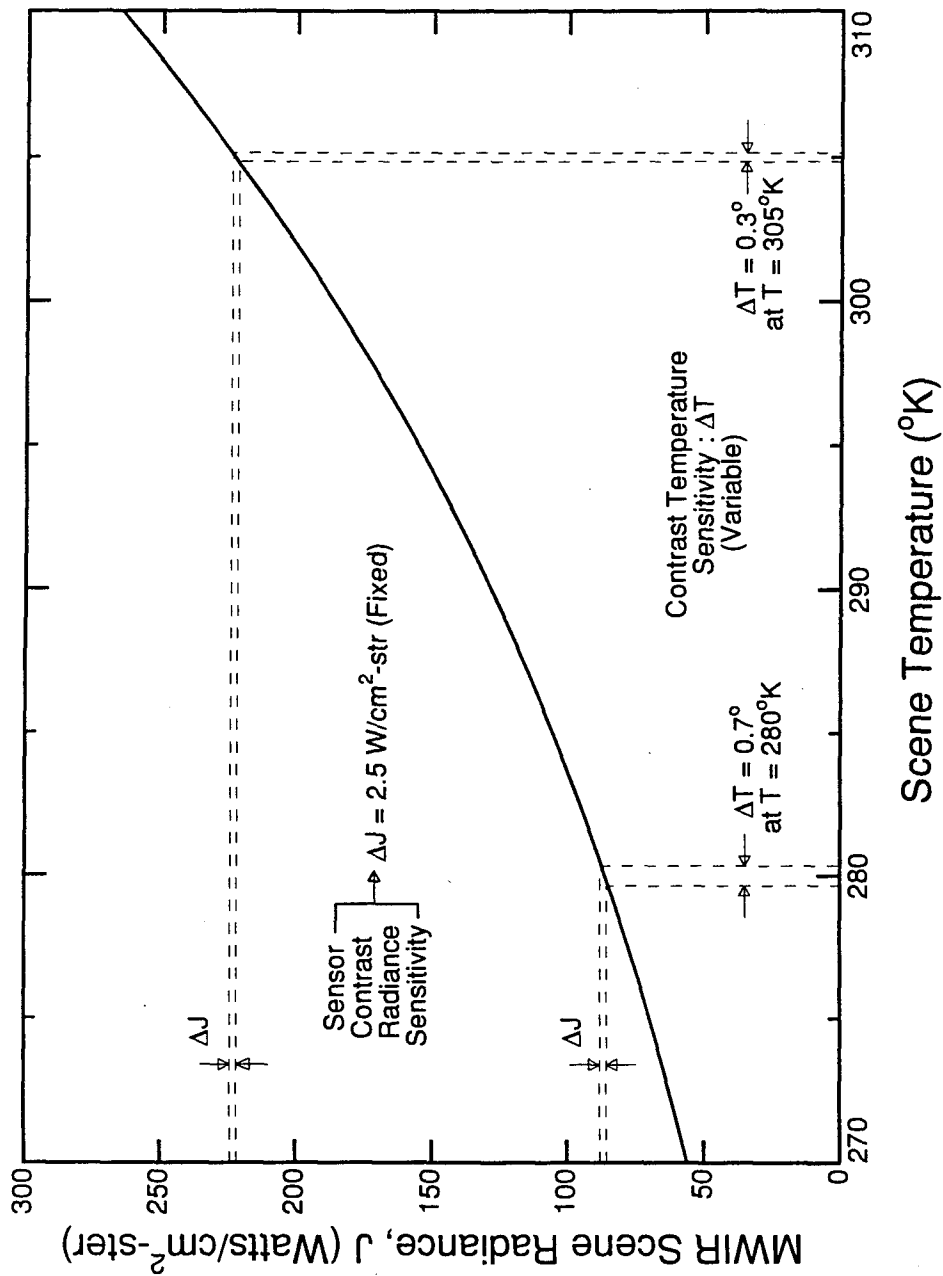


Figure 4-1. The relation of radiometric contrast temperature to measured contrast radiance. The measured radiance values are taken to be from equivalent black bodies and so in a given band,  $\delta\lambda$ , a radiometric temperature can be assigned to a measured radiance.



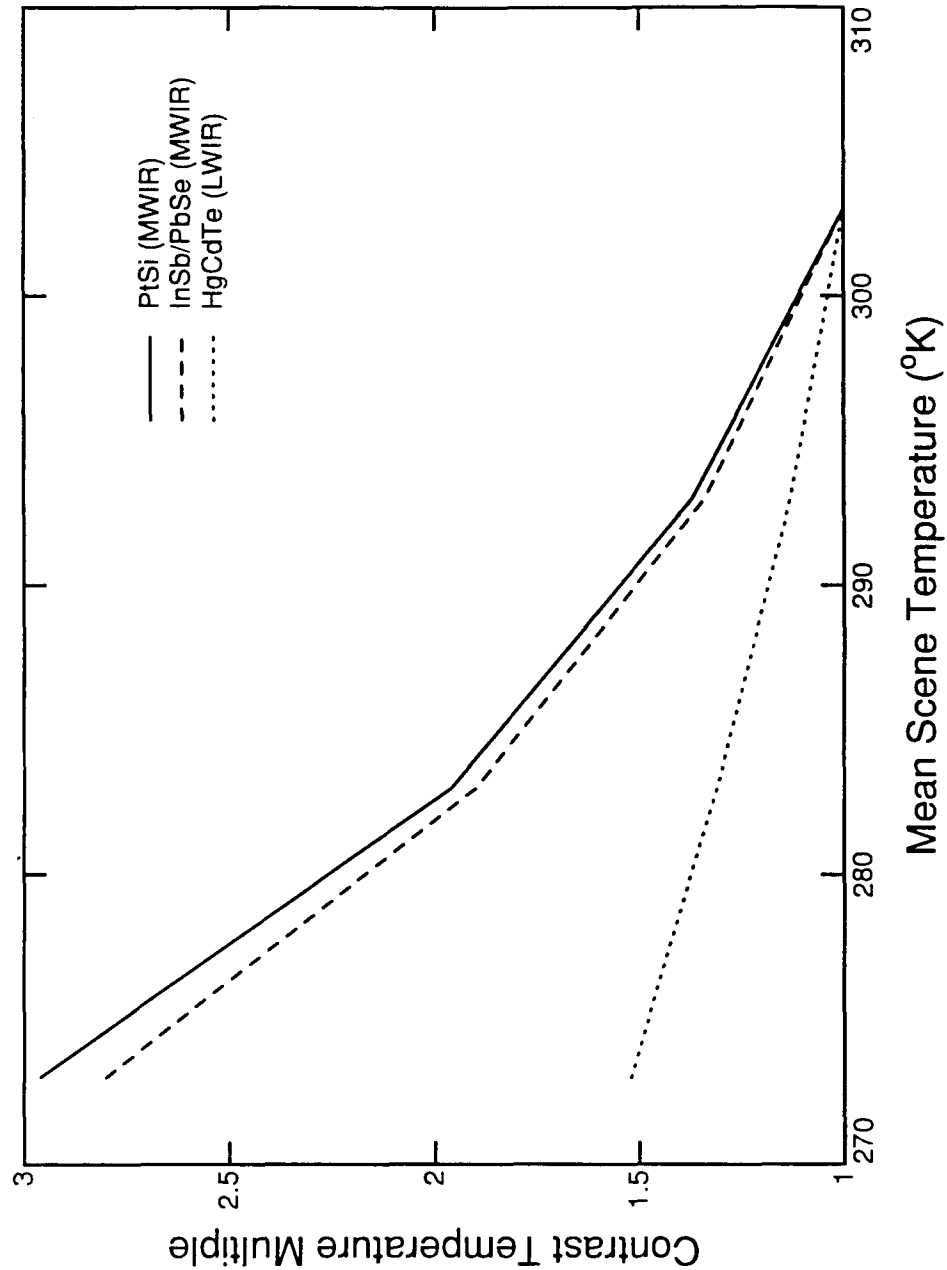


Figure 4-2. The dependence of relative contrast temperature sensitivity on mean scene temperature. An MWIR sensor sensitivity is expressed in contrast temperature (referenced to a specific scene temperature). At a different scene temperature the sensor sensitivity will be different.

array, that is 19,200 detectors, upon which the sensor is built and the high quantum efficiency (~0.7) of the InSb detector material.

**TABLE 4-2**  
**Infrared Imaging Sensors Tested by USCG**

<b>SENSOR</b>	<b>BANDPASS(<math>\mu</math>)</b>	<b>CONTRAST TEMPERATURE SENSITIVITY (<math>^{\circ}</math>C)</b>
WF - 360 TL	8-12	0.11
FLIR 2000	8-12	0.16
THERMOVISION 210	3-5	0.10 @ 16 $^{\circ}$ C (289 $^{\circ}$ K)
IRC - 160ST	3-5	0.04 @ 27 $^{\circ}$ C (300 $^{\circ}$ K)
FSI PRISM	3-5	0.10 @ 30 $^{\circ}$ C (303 $^{\circ}$ K)

## **CHAPTER 5**

### **DATA ANALYSIS AND SENSOR NOISE**

#### **5.1 QUALITATIVE CHARACTER OF DATA**

##### **5.1.1 Caveats**

Before discussing the Coast Guard test data in the framework of the theory of Sections 2, 3, and 4, three points must be made and their implications drawn. First, the data are not calibrated so no quantitative comparison can be made between theory and data. One must rely on stated instrument sensitivities (that is, minimum detectable temperature differences) and make qualitative (or at best semi-quantitative) inferences as to whether a given sensor can detect the contrast temperature difference expected from theory. Second, since some sensitivity may be lost in the transcription process (analog-to-digital) the actual sensitivity floor of the data may not be as good as the manufacturer's values of Table 4-2. Thus there is some uncertainty in sensor input for the data-theory qualitative comparison. Third, brightness and contrast settings, which are made by the operator in real-time, may not have been optimum for a given data pass. Nevertheless, as is now seen, the data does in fact bear out the expectations of Section 3.

##### **5.1.2 Qualitative Summary of Nighttime Observations**

The IR imagery results for infrared nighttime observations can be qualitatively stated in simple terms. The LWIR FLIRs of Table 4-2 can clearly detect an oil-water contrast temperature on both nights (May 4 and 5, 1993) on which data were taken. Neither the Thermovision 210 nor the FSI Prism MWIR FLIR could clearly detect contrast on the night of May 4, and no data were collected with these sensors on the night of May 5. The IRC MWIR FLIR detected a low contrast level on May 5 and, at best, a marginal contrast level on May 4. This behavior, as will be shown, is as expected from the theory of Section 3.

## 5.2 IR IMAGERY DATA AND SENSOR SELECTION

The most important environmental parameters for the LOWTRAN-based contrast calculations of Section 3 are surface temperature and relative humidity. Measured values are given in Table 5-1 for the nights of May 4 and 5. These conditions correspond fairly closely with those for the U.S. summer standard atmosphere: 21°C and 76% relative humidity.

**TABLE 5-1**  
**Measured Environmental Parameters and**  
**Standard Summer Atmospheric Values**

<b>PARAMETER</b>	<b>MID-LATITUDE SUMMER LOWTRAN</b>	<b>MEASURED MEAN: MAY 4</b>	<b>MEASURED MEAN: MAY 5</b>
Temperature (°C)	21	17	21
Relative Humidity (%)	76	68	83

Figure 5-1 is a representative LWIR image for both nights. The layout of the pools and the various types of oil in the pools are detailed in Reference 1. In Figure 5-1 the compass orientation and numbering of the twelve pools which make up the complex is given. For the purposes of this work it is only necessary to note that: tanks 4, 8 and 11 have water only while the other tanks have different types of fresh or weathered oil.

Oil-water contrast is clearly seen in Figure 5-1. Figure 5-2 is an MWIR image taken with the IRC-160 on May 4th; and Figure 5-3 is an image taken with the same sensor on May 5. An oil-water contrast is just seen on May 5 but not on May 4. Figure 5-4 is a digital contrast-enhancement of a different IRC-160ST image taken on May 4. The oil-water contrast can just be seen.

Figures 5-5 and 5-6 are comparisons of predicted water-oil contrast temperatures for various detector materials with the sensitivity levels of the five imagers tested.

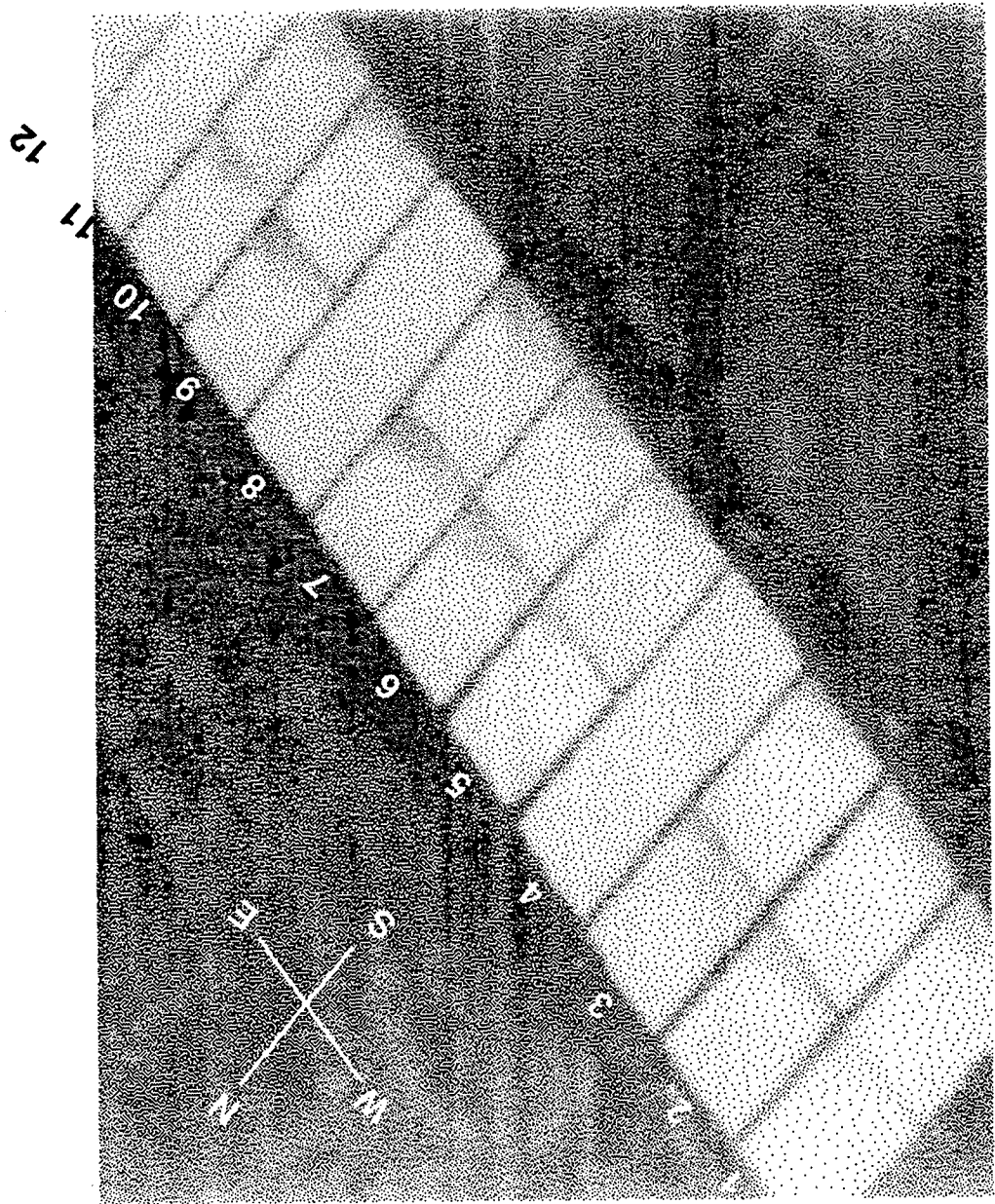


Figure 5-1. Representative nighttime LWIR image of tank complex. "Warmer" areas are whiter. The dark patches of oil are seen in all tanks except 4, 8, and 11 which contain water only.

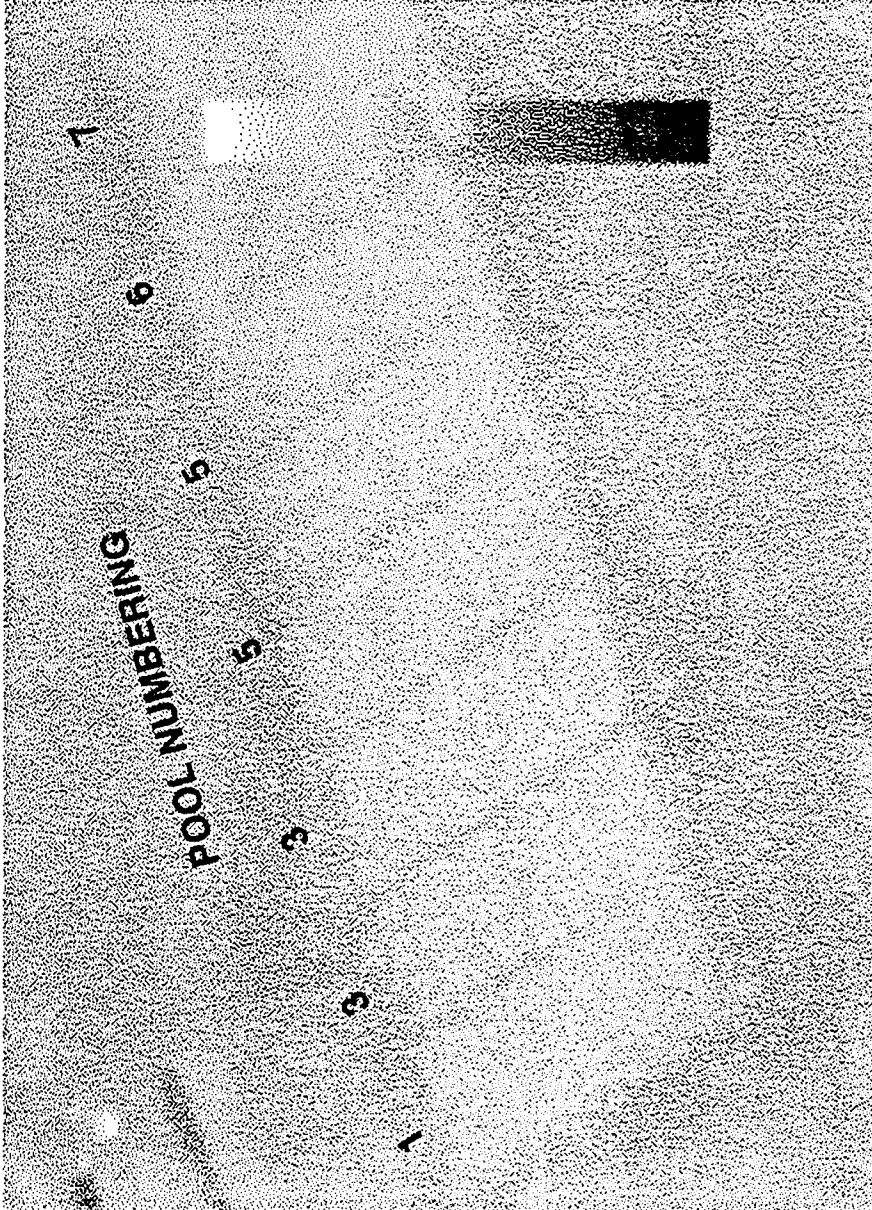


Figure 5-2. Representative MWIR image of tank complex taken with IRC-160ST on night of May 4.  
No contrast in the pools is visible to the eye.

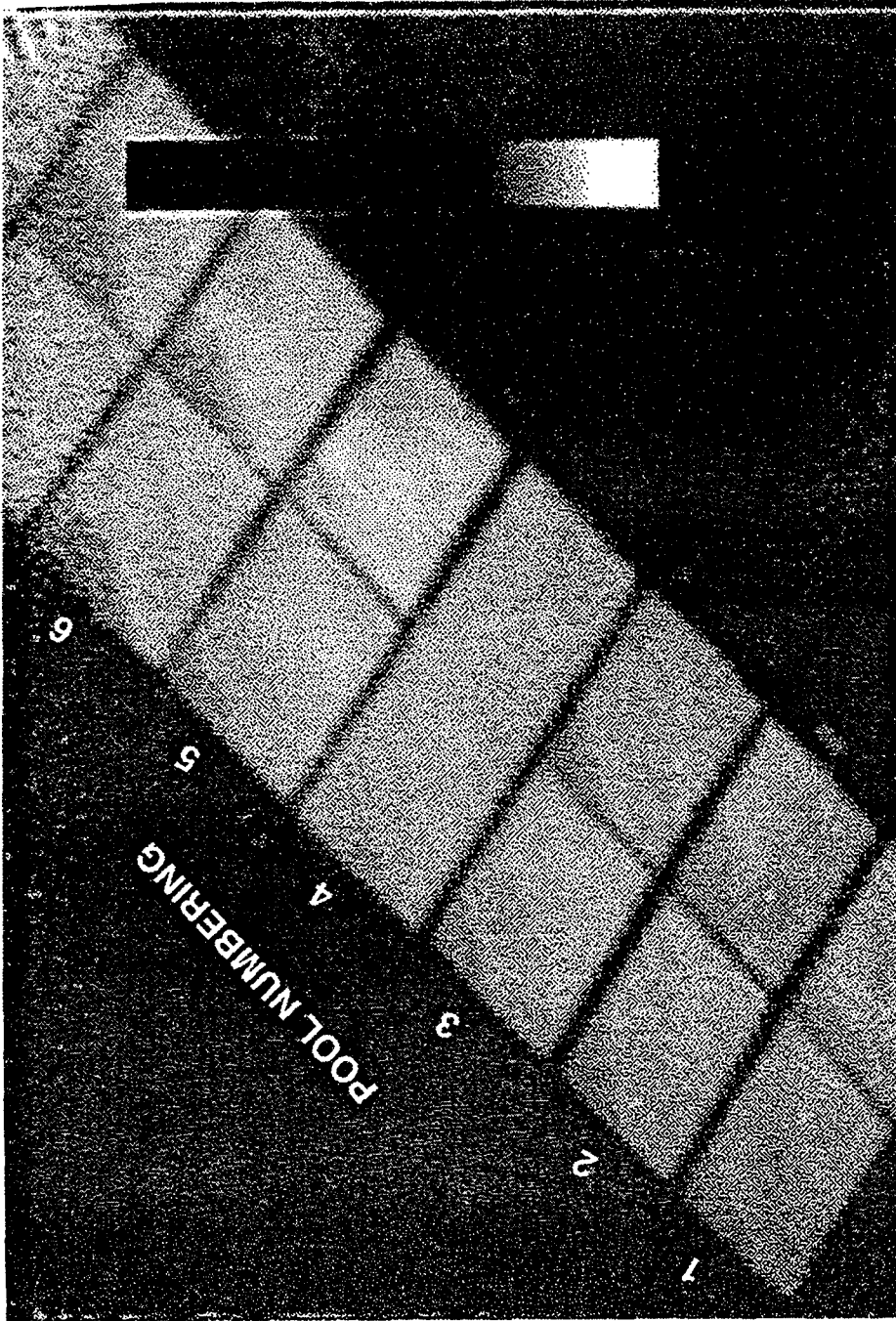
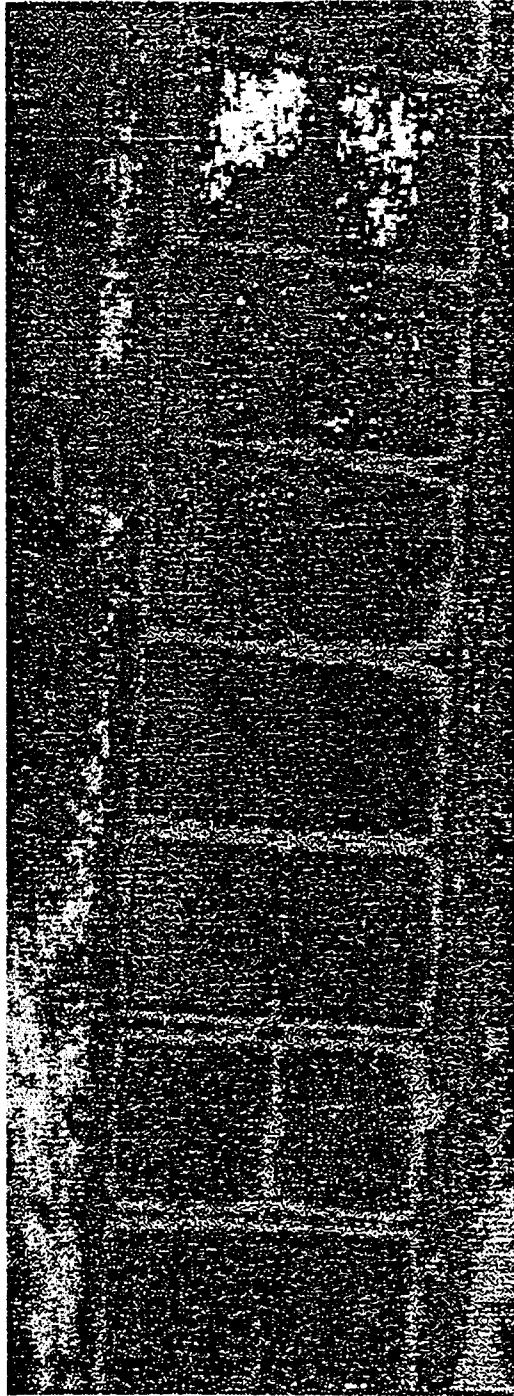


Figure 5-3. Representative MWIR image of tank complex taken with IRC-160ST on night of May 5. "Warmer" areas are lighter. Darker patches of oil are detectable on all tanks except tank 4 which has water only.



1 2 3 4 5 6 7 8

**POOL NUMBERING**

Figure 5-4. A digital gray scale enhancement of a section of the tank complex seen in figure 5-2. Lighter regions are "colder." Water tank (4) is dark but light flecks can be seen in most of the other tanks. This is presumably oil. (IRC-160ST, May 4, 1993)



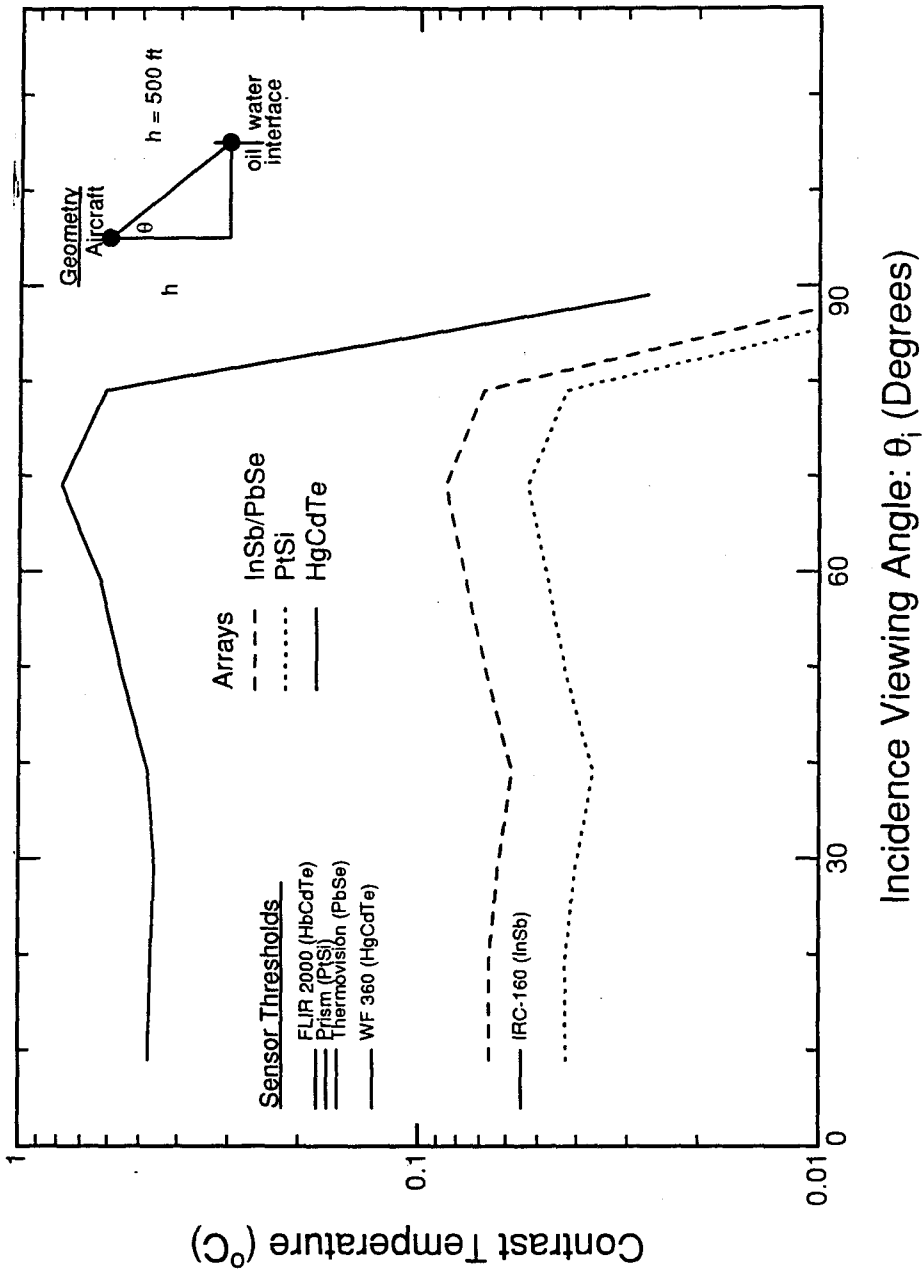


Figure 5-5. Comparison of predicted water-oil contrast temperatures for night of May 4 with sensor thresholds. Sensor sensitivity (horizontal line segment) must be below corresponding material curve for contrast to be detectable.

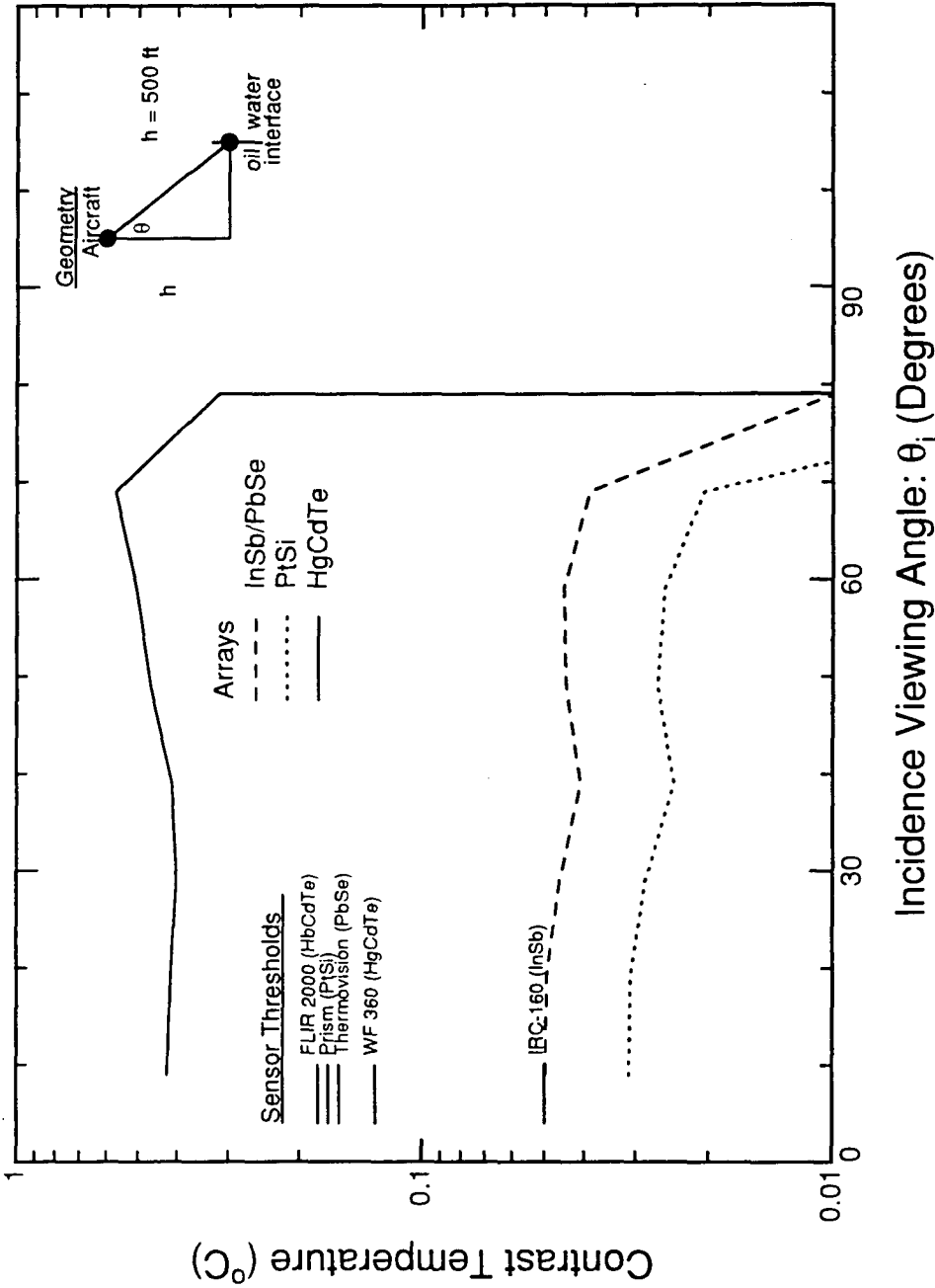


Figure 5-6. Comparison of predicted water-oil contact temperature for night of May 5 with sensor thresholds. Sensor sensitivity (horizontal line segment) must be below corresponding material curve for contrast to be detectable.

Adjustments have been made, using Figure 4-1, for the temperature dependence of the MWIR sensitivities. The predicted curves correspond to the measured meteorological conditions (Table 4-1) on the nights of May 4 and May 5. The sensor sensitivities are indicated by short horizontal bars. For a sensor to detect a contrast temperature its sensitivity (horizontal bar) must be below the corresponding (same detector material) predicted curve. One can see that on both nights the two LWIR FLIRs (WF-360, FLIR-2000) should have (and did) detected a water-oil contrast; neither the PRISM nor the Thermovision MWIR FLIRs should (nor did they) detect a water-oil contrast; and the detection of a contrast with the IRC-160 should be (and was) marginal on both nights. In summary, the semi-quantitative data and theoretical expectations are in agreement, and do allow decisions to be made and justified on the sensor choice for nighttime marine oil slick detection. As a final test we compare in Figure 5-7 predicted contrast temperatures for the LWIR and MWIR for various seasons/latitudes with the sensitivities for the WF-360 LWIR sensor and the IRC-160 MWIR sensor, with sensitivities corrected for scene temperature from Figure 4-2. Once again, one had clear detectability in the LWIR with both LWIR FLIRs, marginal detectability in the MWIR with the state-of-the-art IRC-160. It can be seen in Figure 5-7 that the typical environment is the most favorable for the nighttime detection of oil with the MWIR FLIR.

An LWIR imager would appear to be preferable to an MWIR imager for nighttime spill detection. The WF-360 is somewhat more sensitive than the FLIR 2000 and so, other things being equal, is expected to be the better oil slick imager under stressing (minimal contrast) conditions. The FSI PRISM and Thermovision 210 sensors do not appear to have sufficient sensitivity for reliable nighttime spill detection. The data and analysis presented here are not sufficient to make a complete assessment of the value of the IRC-160 sensor in nighttime spill detection, but this sensor has demonstrated a potential nighttime capability which should be further explored.

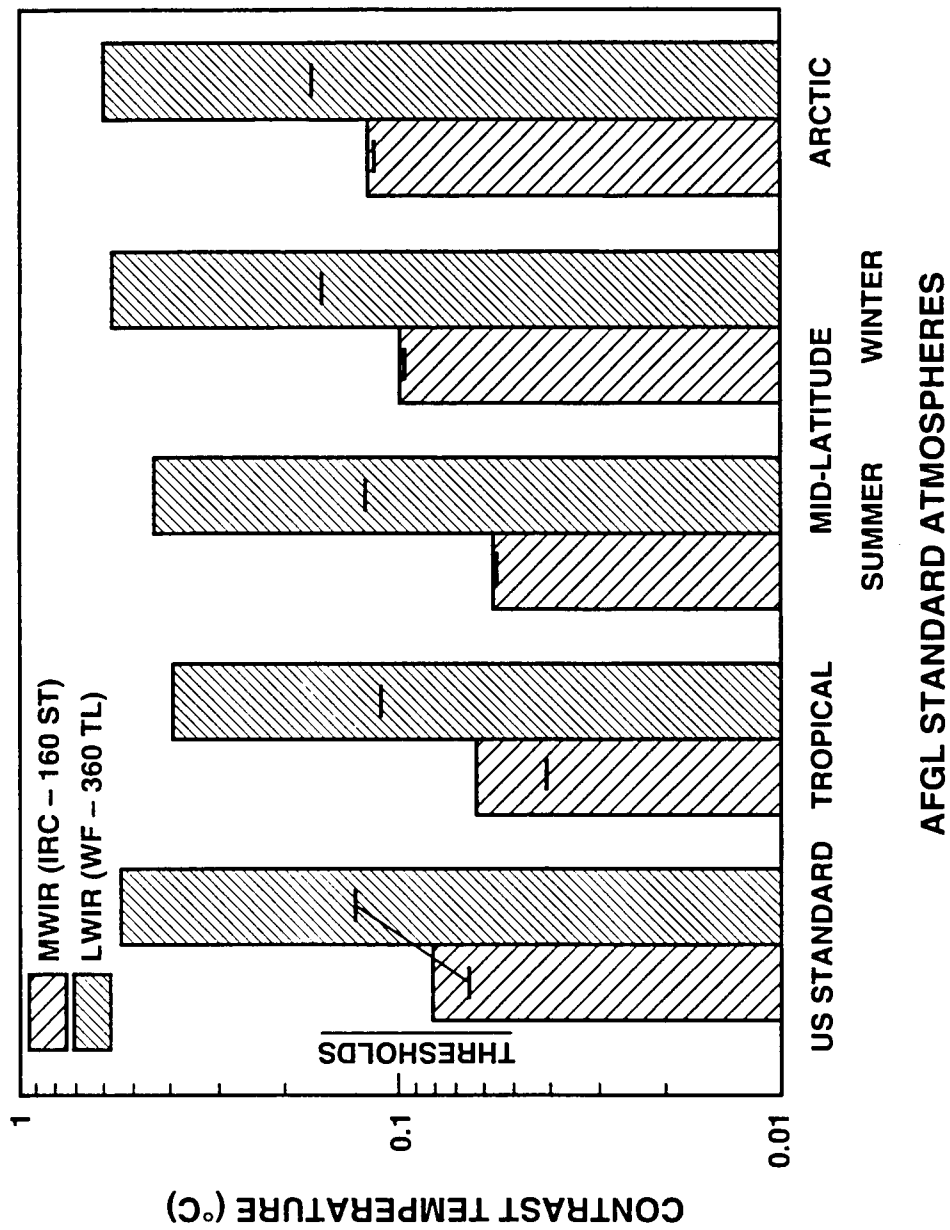


Figure 5-7. The effect of season and latitude on predicted nighttime detectability in the LWIR and MWIR. Sensor thresholds (horizontal line segments) are below predicted contrasts (hatched vertical bars) so oil is detectable.

### 5.3 DAYTIME VIDEO AND NIGHT VISION IMAGERY CRITIQUE

The oil slicks are clearly seen in the daytime as quite dark regions on fairly bright water. Data were taken at night with a night vision camera obtained for the field experiment, [reference 1]. The camera incorporates a state-of-the-art image intensifier tube operating in the visible and near-IR. At night the spills, as shown in Figure 5-8, are easily seen with this sensor as dark regions against fairly bright water. However, if one looks at the lake water, which can be seen in the lower left corner of Figure 5-8, one realizes that caution is needed in drawing inferences on spill detectability. The lake water is quite dark and looks more like the oil in the test tanks rather than the water in the test tanks. The cause of this apparent discrepancy is easy to trace if one reviews Figure 2-11, which displays the penetration depth of water in the visible and near-infrared. The water in the pool is only a few inches deep and so is not optically thick at visible and near-infrared wavelengths. The lake, of course, is optically thick. In both the day video and night vision data one is seeing light reflected from the bottom of the pool. The surface reflectivity of both water and oil in the visible and near-infrared is only a couple of percent. Their contrasts, as now argued, should not be detectable.

Data were obtained on the relative contrast sensitivity of GEN III night vision sensors from Shakpour Ahmadi of the Night Vision and Electronic Sensors Directorate at Fort Belvoir, Virginia. This sensitivity is a function of scene luminance (i.e., brightness) and is plotted in Figure 5-9. The scene luminance is given in foot-lamberts (a conventional unit) and verbal characterizations are added to the curve for ease of interpretation. Without going through relative contrast calculations it is simply noted that the maximum expected oil-water contrast would be a few percent. The nominal sensitivity of the night vision device at the luminance expected from the full moon on the sea is about 10% or greater. One then does not expect to see oil on water at night with current, (GEN-III) night vision sensors under natural illumination. Thus one would not expect to see oil on water at night with current (GEN-111) night vision sensors under natural illumination - *if the reflected natural radiation depended only upon surface reflectivity differences.* However,

as discussed in Section 2.3.2 volume scattering from suspended particulate matter can contribute to backscatter from both oil and water. No general statement on the strengths of these components can be made without detailed knowledge of the volume scattering and absorption properties of the oil and water being observed.

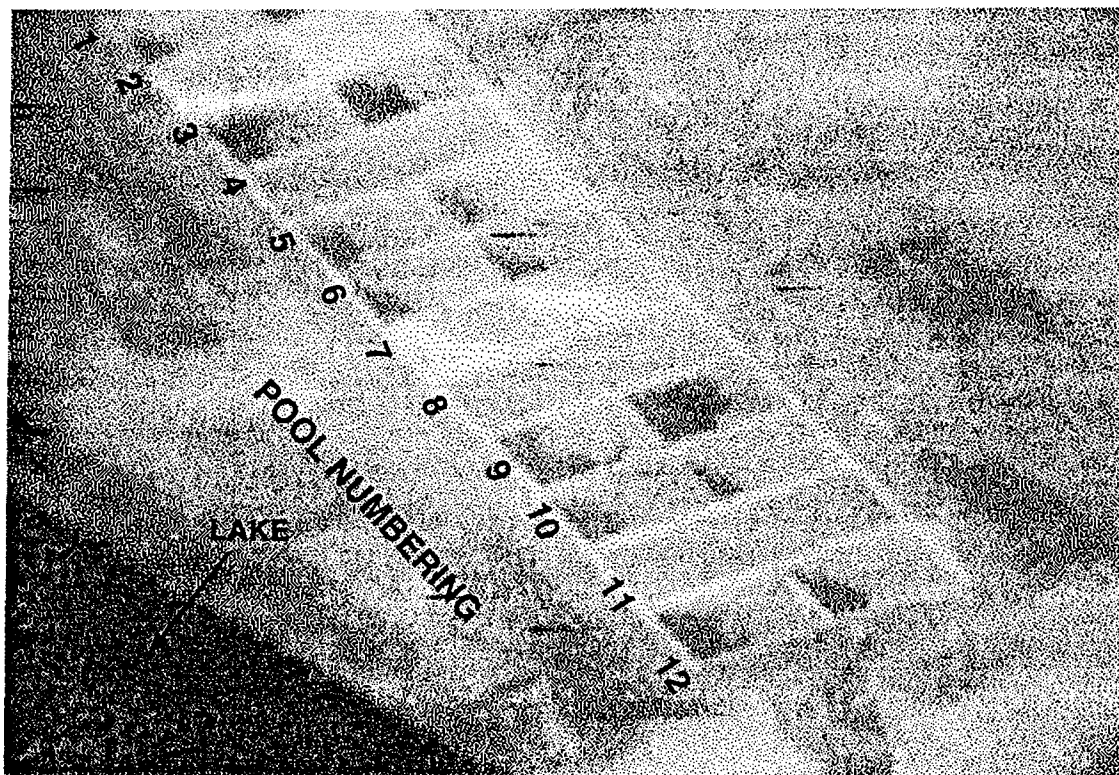


Figure 5-8. Night vision camera image of pool complex.

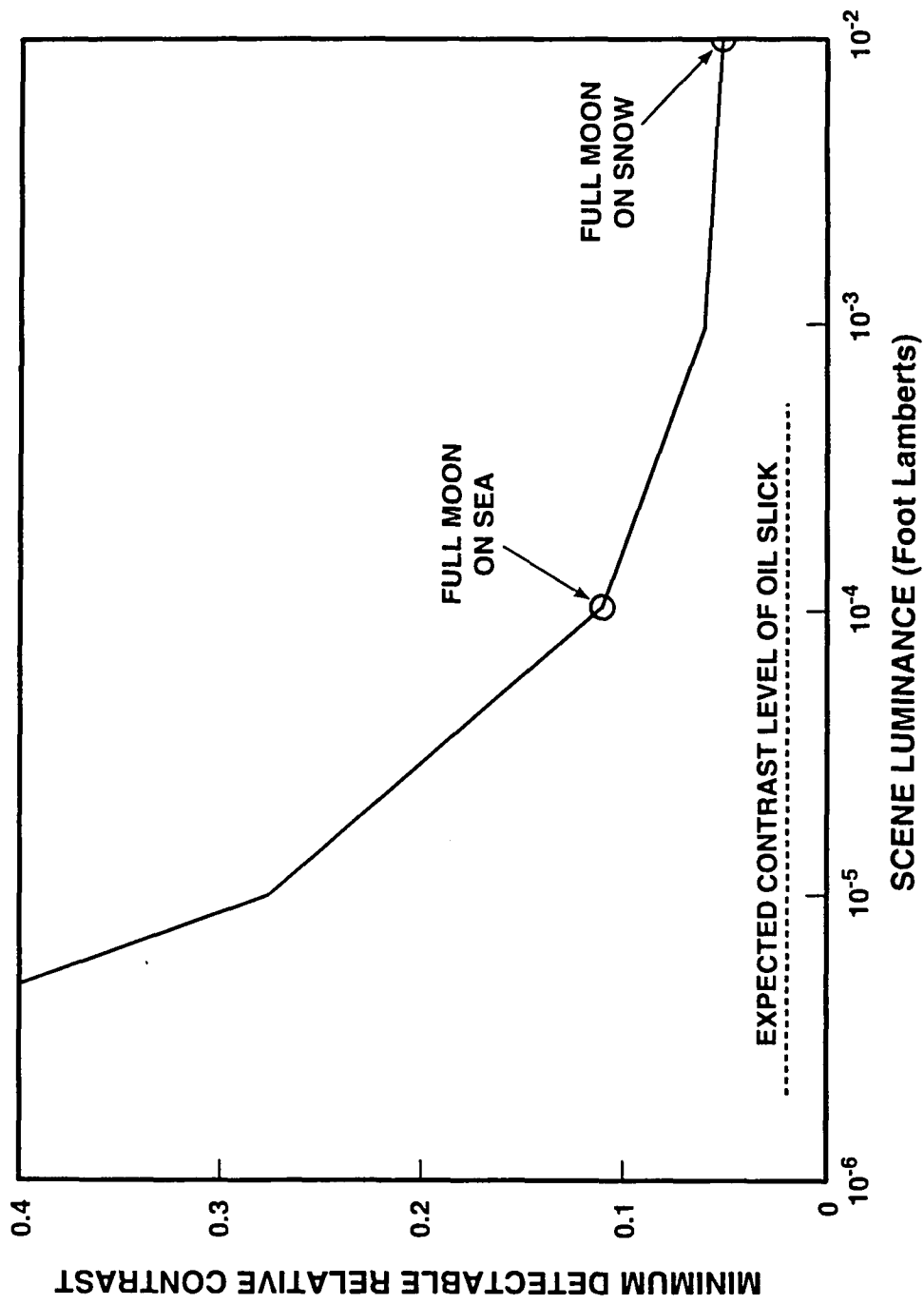


Figure 5-9: Relative contrast detectable with GEN III device. At maximum illumination level (full moon) on sea minimum detectable contrast is much greater than expected oil slick contrast. Expected contrast is estimated from surface reflectance only; could be enhanced by volume scattering (see text).



## **CHAPTER 6**

### **RECOMMENDATIONS**

#### **6.1 SENSOR RECOMMENDATIONS**

Imaging sensors operating in the LWIR band (8-12 microns) are preferred over those operating in the MWIR band (3-5 microns) for the nighttime detection of oil spills at sea. This conclusion is based upon the theoretical analysis of this report and supported, qualitatively, by the field test data presented in Chapter 5. The physical reason for the greater radiometric temperature contrast seen in the LWIR (relative to the MWIR) can be traced to Table 2-1 and Figure 2-4. The primary driver of the IR contrast signature is the oil-water emissivity difference. This difference is seen to be uniformly larger for the 8-12 micron band compared to the 3-4 and 4.5-5.5 micron bands. The specific calculations of this analysis used the most stressing oil type in Table 2-1 and are, in effect, slightly biased against MWIR sensors because the MWIR emissivity difference are particularly small. The general statement just made, however, holds.

No usable data were obtained during the field test for the evaluation of night vision imagers. However, theoretical calculations strongly suggest the current systems (Gen-III technology) are not sufficiently sensitive to detect oil spills at night using natural illumination.

#### **6.2 FURTHER WORK**

There are three areas, suggested by this analysis, which should be more fully explored in the context of nighttime spill detection. First, calibrated data on IR imagery of controlled nighttime spills should be obtained. This data should be digitally recorded at the full sensitivity (~ 10 bits) of the various IR images. Calibrations could be made with controlled test targets in the imaged scenes. Data prediction comparisons such as those of Figure 5-5, then could be made quantitatively.

Second, a paper study should be made assessing the value to spill detection of the low-noise CCD arrays now being developed, [reference 19]. They should be both inherently more sensitive than GEN-III devices and, at production levels, less expensive. Their contrast sensitivity depends upon available integration time and so the details of spill extent and aircraft motion. A system study is needed here.

Third, data on IR absorption of oils are needed in the MWIR and LWIR, to fully support the assumptions of this analysis. Further, this requirement, when met, would allow a quick feasibility assessment of some sort of differential absorption measurement to estimate oil spill thickness probably in the 0.01-0.1 millimeter thickness range. In the vicinity of an absorption band the absorption of an oil layer would vary sharply with wavelength. The amount of variation would depend upon oil layer thickness. In principle, measurements at many closely spaced wavelengths (e.g., with a tunable laser) could allow inferences to be drawn on spill thickness.

Finally, and separate from the above, the evaluation of the relative value of state-of-the-art MWIR and LWIR FLIRs for daytime use should be continued. This evaluation includes: sensor sensitivity and dynamic range together with spill signature phenomenology. The key sensor parameters here are sensitivity and dynamic range. A sensor that combines these (as the IRC-160ST does) would produce images with a high capability for gathering imaging information on oil spills and the features on the ocean surface as noted in Section 2.3.4. Such a capability might be particularly valuable against thin (a few microns thick) oil films.

## REFERENCES

1. Hover, G.L. and Plourde, J.V., Evaluation of Night-Capable Sensors for the Detection of Oil on Water, U.S.Coast Guard Research and Development Center March 1994.
2. Brown, E. et. al., Design, Construction, Test, an Evaluation of a Frequency Scanning Radiometer for Measuring Oil Slick Thickness, M.I.T. Lincoln Laboratory, Lexington, Mass., Final Report, June 1994.
3. Skou, N., "Microwave Radiometry for Oil Pollution Monitoring Measurements and Systems," IEEE Trans. Geo. Sci. GE-24, 3, 360, May 1986.
4. Lodge, A.E., ed. The Remote Sensing of Oil Slicks, J. Wiley, 1989.
5. Salisbury, J.W., et. al., "Thermal Remote Sensing of Crude Oil Slicks," Remote Sens. Environ., 45, 225, August 1993.
6. Hollinger, J.P., The Determination of Oil Slick Thickness by Means of Multifrequency Passive Radiometric Techniques, U.S.C.G., No. CG-D-31-75, ORD, 1974.
7. Hoyer, J.E., "Oil Film Thickness Using Airborne Laser-Induced Oil Fluorescence Backscatter," Appl. Opt., 22, 3316, 1983.
8. Ulaby, F.T., et. al., Microwave Remote Sensing, Vo. 3, 1467a, Artech House, 1986.
9. Goody, R.M., Young, Y.L., Atmospheric Radiation, Oxford University Press, 1989.
10. Born, M., Wolf, E., Principles of Optics, Chapter 1, Pergamon Press, 1975.
11. Horvath, R., et. al., Optical Remote Sensing of Oil Slicks: Signature Analysis and Systems Evaluation, University of Michigan, prepared for U.S. C.G., 1971.
12. Cox, C., Munk, W.,: Measurement of the Roughness of the Sea from Photographic of the Sun's Glitter," J.O.S.A., 44, 838, 1954.
13. Derr, V.E., "Remote Sensing of the Troposphere," NOAA, No. C55602775, August 1972.
14. Wolfe, W.L., ed. The Infrared Handbook, Chapters 1 and 3, ERIM, ONR, 1975.

## REFERENCE (CONTINUED)

15. Kniezys, F.X., et. al., Users Guide to LOWTRAN 7, AFGL-TR-88-0177, AFGL, 1988.
16. Ewing, G.C., McAlister, E.D., "On The Thermal Boundary Layer of the Ocean," Science 131, 1374, May 6, 1960.
17. Ewing, G.C., ed. Oceanography from Space, Woods Hole Oceanographic Institute., WH 01, No 65-10 April 1965.
18. Eagleson, P.S., Dynamic Hydrology, Chapter 14, McGraw Hill, 1970.
19. Burke, B., "Abutable CCD Imager for Visible Focal Plane Array," IEEE Trans. on Elect. Inst., 38, 1069, May 1991.